ELSEVIER

Contents lists available at ScienceDirect

# International Journal of Pharmaceutics

journal homepage: www.elsevier.com/locate/ijpharm





# Ultrasonic characterization of complete anisotropic elasticity coefficients of compressed oral solid dosage forms

Tipu Sultan <sup>a</sup>, Shubhajit Paul <sup>b</sup>, Enamul Hasan Rozin <sup>a</sup>, Christian Canino <sup>a</sup>, Yin-Chao Tseng <sup>b</sup>, Cetin Cetinkaya <sup>a,\*</sup>

- a Department of Mechanical and Aeronautical Engineering, Photo-Acoustics Research Laboratory, Clarkson University, Potsdam, NY 13699-5725, USA
- b Material and Analytical Sciences, Boehringer Ingelheim Pharmaceuticals, Inc, Ridgefield, CT 06877, USA

#### ARTICLE INFO

Keywords:
Anisotropy in compacts
Transversely isotropic materials
Constitutive relations
Solid dosage compacts
Ultrasonic evaluation
Non-destructive characterization/evaluation
techniques

#### ABSTRACT

In compacted materials, elastic anisotropy coupled with residual stresses could play a determining role in the manifestation of various types of defects such as capping and lamination, as it creates shear planes/bands and temporal relaxation. This internal micro-structure leads to time-delayed flaw initiation/formation, crack tip propagation under residual stresses, and ultimately product quality failures. Thus, their accurate characterization and variations are useful for understanding underlying failure mechanisms and to monitor variations in materials, processes and product quality during production prior to onset of failure. The extraction of tablet anisotropic elasticity properties is a challenging task, especially for commercial tablets with complex shapes, as shape often prevents the use of traditional destructive techniques (e.g., diametric compression testers) to produce accurate measurements. This study introduces and applies an ultrasonic approach to extracting the complete transverse isotropic elastic properties of compressed oral solid dosage forms to a commercial tablet product. A complete set of waveforms and the constitutive matrix for the compacted materials are reported. In addition, a perturbation analysis is carried out to analytically relate propagation speeds in various directions to the elastic coefficients. The proposed characterization approach is non-destructive, rapid, easy, and reliable in evaluating tablet anisotropy.

# 1. Introduction

Today the vast majority of medicines administered to a patient are Oral Solid Dosage Forms (OSDF), where Active Pharmaceutical Ingredient(s) (APIs) is/are combined with a range of excipients through a sequence of processes that allow manufacturability, ease of use, and the targeted therapeutic effect. Throughout its manufacturing process, the safety and efficacy of an OSDF product are maintained through a strict control strategy. In the production process, it is critical to detect/measure/sense, control, and monitor any sources of material, process, and machinery variations affecting the Critical Quality Attributes (CQAs) of an OSDF product. At present, due mainly to productivity and supply chain stability requirements, the pharmaceutical manufacturing technologies for compressed OSDF (tablets) are rapidly converging into two key technologies: Continuous Manufacturing (CM) and Real-Time Release (RTR) testing. In the last decade or so, considerable advances have been made in process analytical technologies, automation, and

digital manufacturing, which paved the way for RTR to eliminate all, or certain, off-line end-product tests assuring that the required quality of OSDF products is achieved.

In recent years, in addition to the extraction of tablet elastic properties, the tablet tensile strength and porosity (Razavi et al., 2016; Xu et al., 2018a) and capping risk (Paul et al., 2021; Paul and Tseng, 2021; Xu et al., 2018b) as well as punch head profile and compaction speeds (Xu et al., 2020) are successfully correlated to the ultrasonically-acquired elastic properties of an OSDF product. Furthermore, a commercial ultrasonic system based on the issued patents (Cetinkaya, 2019, 2017, 2014) for in-die ultrasonic monitoring system has also been commercialized (Kern et al., 2022).

The tensile strength of a tablet is a critical attribute, as it needs to be mechanically strong enough to withstand further handling loads such as coating, branding, packaging, transport and end-use by the patient, but sufficiently soft to disintegrate in the human body to release the API at a prescribed rate. In destructive tests used in practice today, closed-form

<sup>\*</sup> Corresponding author at: Pharmacoustics Technologies, LLC, USA.

E-mail addresses: sultant@clarkson.edu (T. Sultan), shubhajit.paul@boehringer-ingelheim.com (S. Paul), rozine@clarkson.edu (E. Hasan Rozin), caninocg@clarkson.edu (C. Canino), ccetinka@clarkson.edu (C. Cetinkaya).

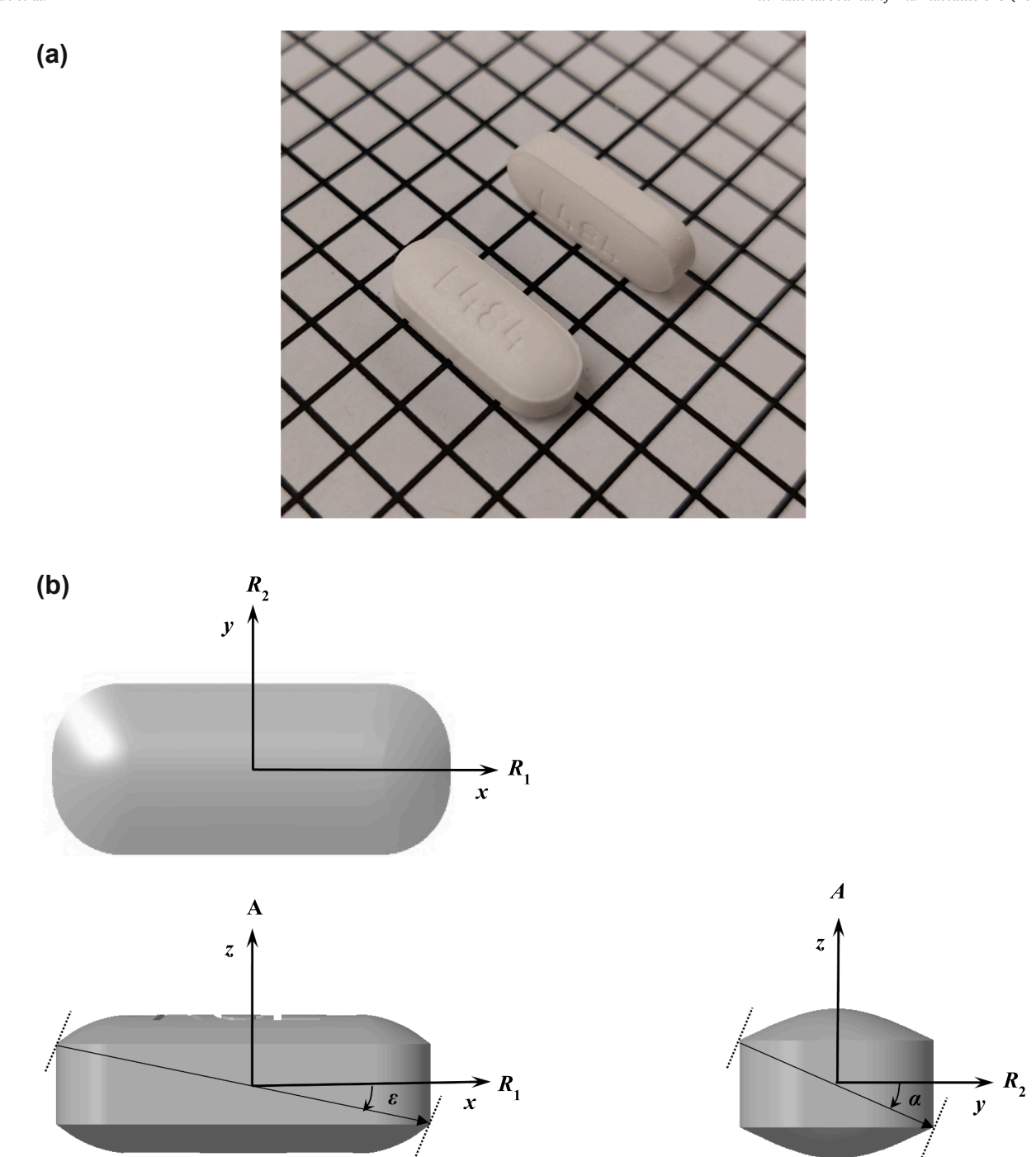
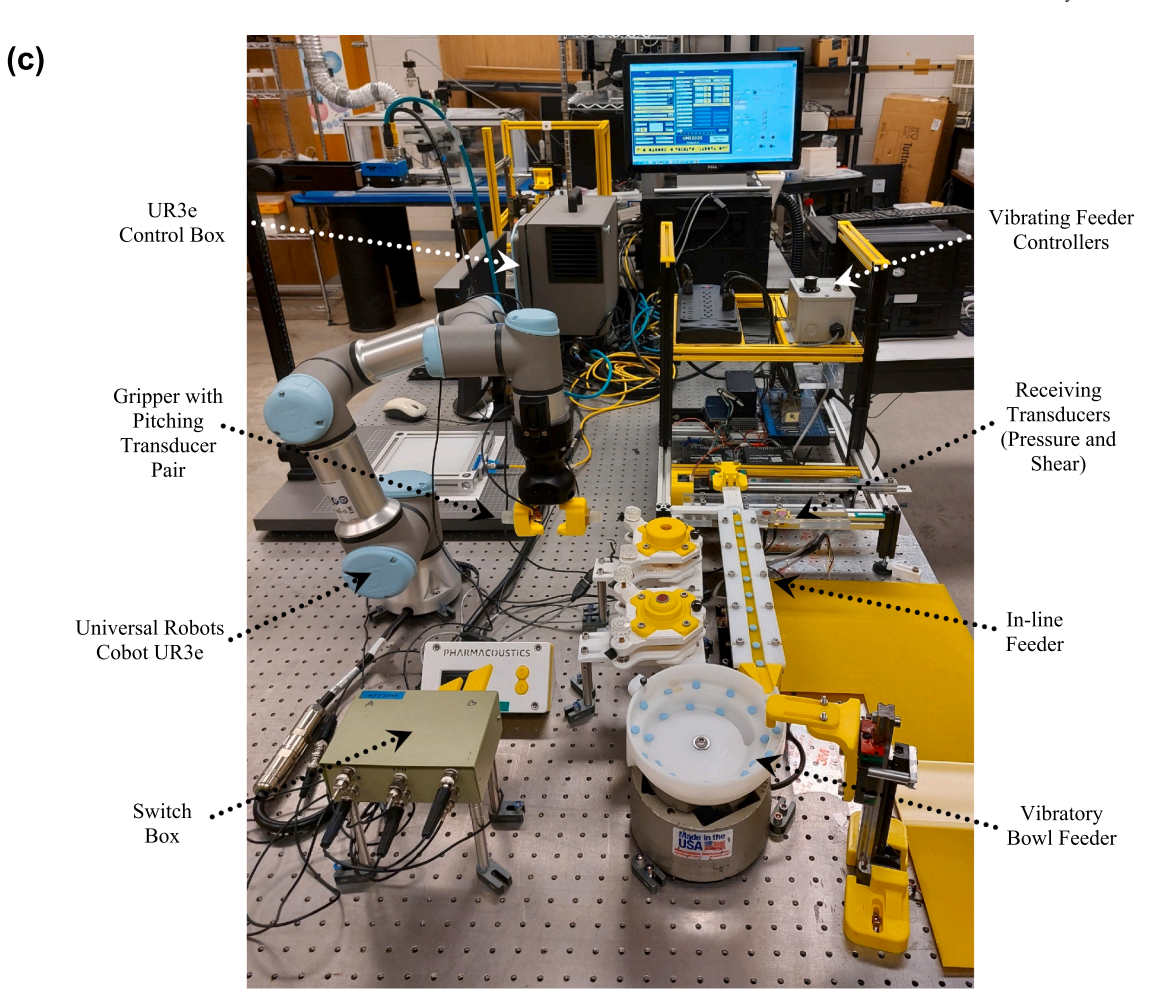


Fig. 1. (a) Image of a commercially available Acetaminophen (Amazon Basic Care) (ACE10) tablet. Background grid: 5 mm by 5 mm. (b) Tablet dimensions and principal axes/wave propagation directions (axial (A): major radial ( $R_1$ ): minor radial ( $R_2$ ): (3)), cross-diagonal (D) major (1), and cross-diagonal (D) minor (2) are as shown. (c) Image of the automated ultrasonic testing system utilized in the experiments (CTF 2022). (d) Schematic diagram of the CTF 2022 rig.

mathematical solutions to determine tensile strength from the fracture load are utilized for flat-faced and convex-faced circular tablets (Pitt and Heasley, 2013). While diametrical compression tests are used for this objective, the determination of tablet strength in a radial direction is often complicated, especially for complex tablet shapes, due mainly to stress concentration on intricately-shaped tablets and the brittle nature of tableting materials. Furthermore, it is known that tablet materials are strongly anisotropic (Akseli et al., 2009; Meynard et al., 2021; Mullarney and Hancock, 2006), which limits the use of closed-form mathematical

solutions developed for regular isotropic shapes.

In its elastic/plastic deformations, a tablet records the stress-state experienced during compaction and it is now well established that tensile strength correlates to elastic properties (Razavi et al., 2016; Xu et al., 2018a); thus, it might be possible to non-destructively predict its fracture load from elastic properties if such properties are accurately extracted. Furthermore, strain localization during compaction leads to the formation of shear bands, and defects as well as anisotropy. The anisotropy of tensile and compressive strengths may be associated with



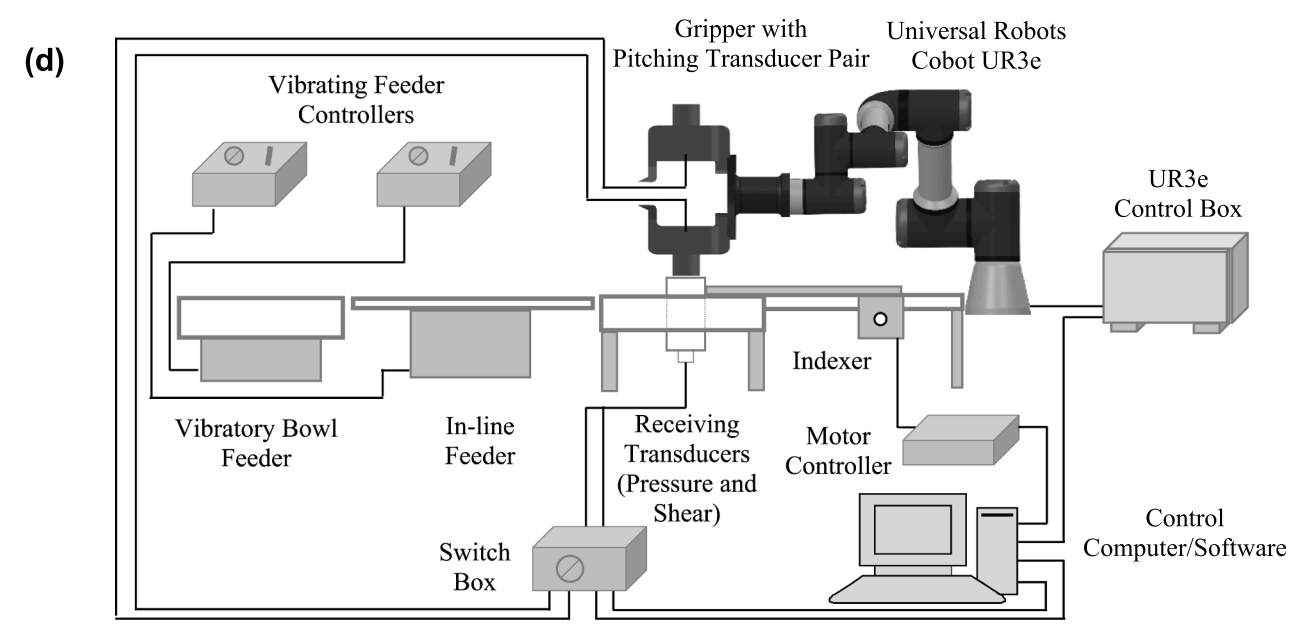
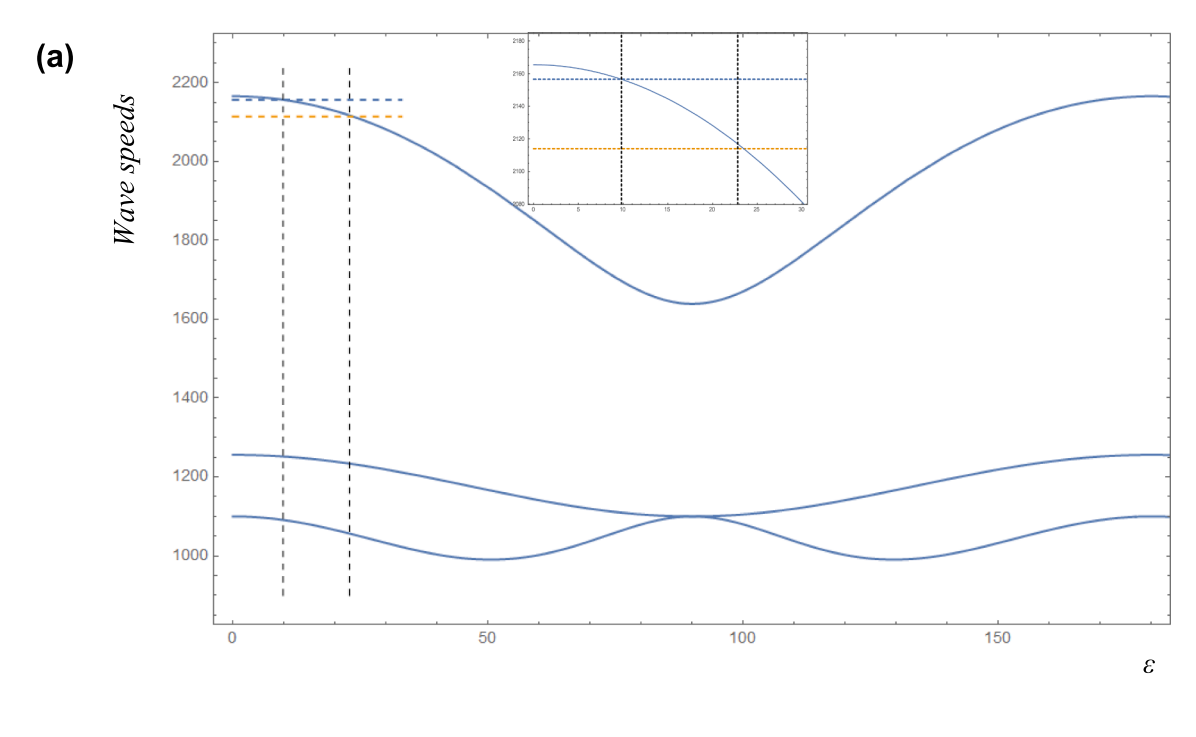


Fig. 1. (continued).

different failure modes and deformation mechanisms, depending on how stress is applied relative to the anisotropy planes (Baud et al., 2005)

Researchers demonstrated the use of an impulse excitation method to determine the anisotropy of flat-faced cylindrical tablets (Akseli et al.,

2009; Meynard et al., 2021). Since there is no closed-form expression to calculate the elastic constants using the natural frequencies in the anisotropic case, Finite Element Method (FEM) was used as previously introduced and utilized (Akseli et al., 2010; Akseli and Cetinkaya, 2008) for air-coupled acoustics. Furthermore, it is reported that the ultrasonic



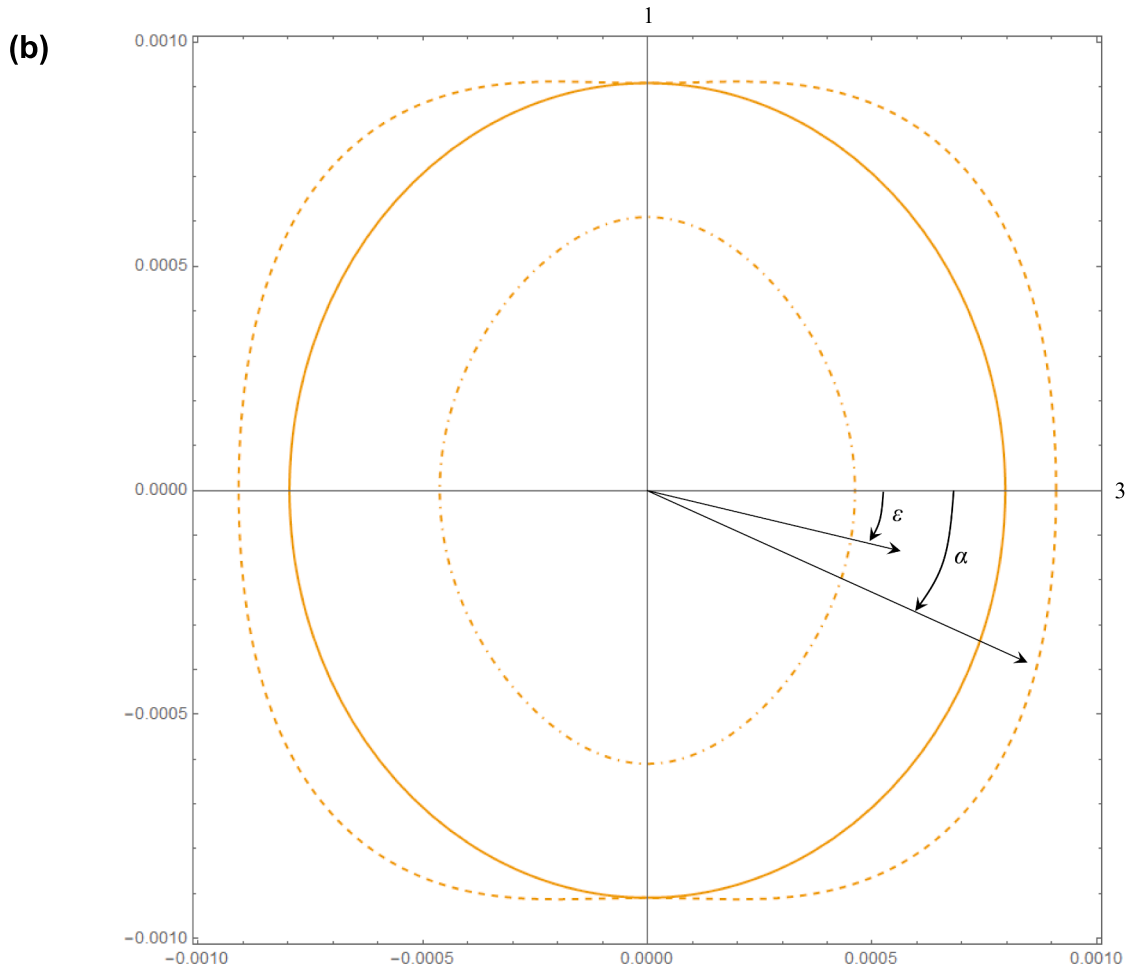


**Fig. 2.** (*a*) Pressure (*L*) (top line) and two shear (*T*) wave (two bottom lines) speeds in an anisotropic tablet material as a function of propagation direction angle ε. Inset: Close-up of the solution for  $c_L$  at the angle ε. (*b*) Slowness diagram of the propagating wave modes on the axial (3)-major (1) axis plane (the directions for the diagonal propagation are marked by arrows for angles ε and α). Slowness is the inverse of velocity. (*c*) Placement of an ACE samples along the radial major diagonal measurement axis with the aid of a specially designed and 3D-printed mold.

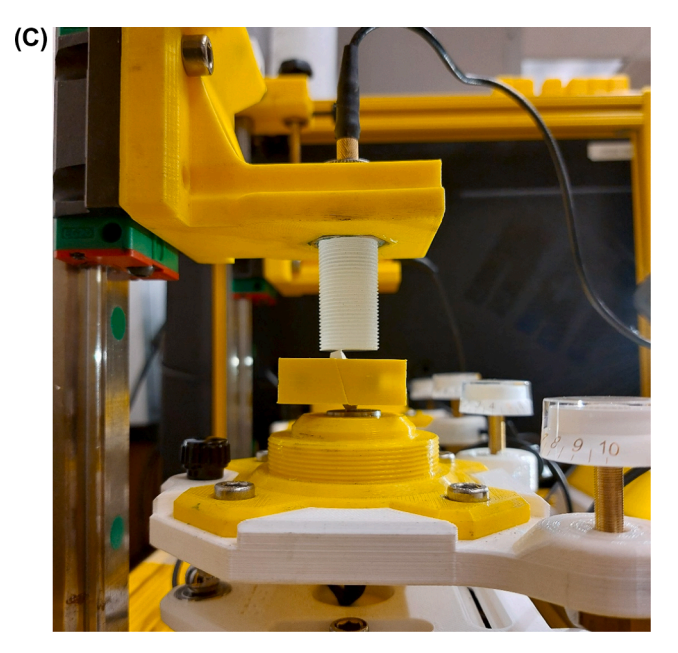


Fig. 2. (continued).

approach was applied in several articles to determine the elastic properties in two perpendicular directions to predict tablet capping tendency (Akseli et al., 2014, 2013, 2009; Xu et al., 2018b).

The full/complete transverse isotropic elastic matrix requires five parameters:  $c_{11}$ ,  $c_{13}$ ,  $c_{33}$ ,  $c_{44}$ , and  $c_{66}$ , and only four elastic wave speeds in the principal coordinates of a sample can be acquired from time-of-flight information in two directions (Auld, 1990). Namely, as shown below, with the measurements in the principal directions, all except  $c_{13}$  can be extracted. In the current work, we present an ultrasonic approach for multi-axis measurements and demonstrate its utility as to how additional off-axis ultrasonic measurements can be made and utilized in determining  $c_{13}$ .

### 2. Mathematical formulation

Compressed OSDF tablets are plastically-deformed transversely isotropic (tiso) materials due to the axial punch-die compaction configuration utilized in their production. First, we present a mathematical framework utilized in the extraction of the complete transverse isotropic elastic matrix entries, namely,  $c_{11}$ ,  $c_{13}$ ,  $c_{33}$ ,  $c_{44}$ , and  $c_{66}$ . For an elastic material, the (wave) dispersion relations as functions of the propagation direction cosines  $(l_x, l_y, l_z)$ , the radial propagation frequency  $(\omega)$ , directional wave number vector  $\overrightarrow{k} = k (l_x \overrightarrow{i} + l_y \overrightarrow{j} + l_z \overrightarrow{k})$  where k is the directional wavenumber, and material properties are obtained from the Christoffel equation, resulting in an eigenvalue problem in the displacement field v and corresponding normalized frequency (Auld, 1990):

$$k^2 \Gamma_{ij} v_j = \rho \, \omega^2 v_i \Rightarrow \Gamma_{ij} v_j = \rho \left(\frac{\omega}{L}\right)^2 v_i$$
 (1)

where  $\rho$  is the material mass density.

$$\Gamma_{ij} = l_{iK} c_{KL} l_{Lj} \text{ with } l_{iK} = k \begin{bmatrix} l_x & 0 & 0 & 0 & l_z & l_y \\ 0 & l_y & 0 & l_z & 0 & l_x \\ 0 & 0 & l_z & l_y & l_x & 0 \end{bmatrix} \text{ and } l_{Lj} = [l_{iK}]^T,$$

and [C] ( $c_{KL}$  in indicial notation) is the constitutive (stiffness) matrix. For purely isotropic (iso) and transversely isotropic (tiso) materials, respectively, the following symmetric matrix forms are used:

$$[C]^{iso} = \begin{bmatrix} c_{33} & c_{33} - 2c_{44} & c_{33} - 2c_{44} & 0 & 0 & 0 \\ & c_{33} & c_{33} - 2c_{44} & 0 & 0 & 0 \\ & & c_{33} & 0 & 0 & 0 \\ & & & c_{44} & 0 & 0 \\ & & & & c_{44} & 0 \\ & & & & & c_{44} \end{bmatrix}$$

$$[C]^{\mathit{tiso}} = \begin{bmatrix} c_{11} & c_{11} - 2c_{66} & c_{13} & 0 & 0 & 0 \\ & c_{11} & c_{13} & 0 & 0 & 0 \\ & & c_{33} & 0 & 0 & 0 \\ & & & c_{44} & 0 & 0 \\ & & & & c_{66} \end{bmatrix}$$

As observed in these forms, the three of the iso material constants are altered by three  $\Delta$  terms to represent the tiso material with an axisymmetric in the z-direction (or direction 3) (Fig. 1.a-b). Thus,  $[C]^{tiso}$  is expressed in terms of  $[C]^{iso}$  and its variations  $\Delta c_{13}$ ,  $\Delta c_{33}$ , and  $\Delta c_{66}$  from the iso case, as follows:

$$c_{33} = c_{33} + \Delta c_{33} = c_{11} + \Delta c_{33}$$

$$c_{66} = c_{66} + \Delta c_{66} = c_{44} + \Delta c_{66}$$

$$c_{13} = c_{13} + \Delta c_{13} = (c_{33} - 2c_{44}) + \Delta c_{13} = c_{12} + \Delta c_{13}$$

$$c_{12} = c_{11} - 2c_{66} = c_{11} - 2(c_{44} + \Delta c_{66}) = c_{11} - 2c_{44} - 2\Delta c_{66} = c_{12} - 2\Delta c_{66}$$

Note that these three  $\Delta$  variational terms also represent the degree-of-anisotropy in the material, as they are measures of deviations from isotropy. In relation to  $[C]^{\mathrm{iso}}$ ,  $[C]^{\mathrm{tiso}}$  is then represented as follows, which provides a means to quantify the degree of anisotropy in a material with respect to its iso counterpart:

$$C^{tiso} = \begin{bmatrix} c_{11} & c_{12} - 2\Delta c_{66} & c_{12} + \Delta c_{13} & 0 & 0 & 0\\ & c_{11} & c_{12} + \Delta c_{13} & 0 & 0 & 0\\ & & c_{11} + \Delta c_{33} & 0 & 0 & 0\\ & & & & c_{44} & 0 & 0\\ & & & & & c_{44} + \Delta c_{66} \end{bmatrix}$$
(3)

The dispersion relations are determined from the characteristic equation roots of the Christoffel equation (Eq. (1)) in the axial (A) direction (z) (0, 0, 1), and the corresponding phase speeds are given as follows:

$$\left\{\omega = \pm \left(\sqrt{\frac{c_{33}}{\rho}}\right)k \Rightarrow c_L = \sqrt{\frac{c_{33}}{\rho}}\right\}$$

$$\left\{\omega = \pm \left(\sqrt{\frac{c_{44}}{\rho}}\right)k \Rightarrow c_T = \sqrt{\frac{c_{44}}{\rho}}\right\}$$

$$\left\{\omega = \pm \left(\sqrt{\frac{c_{44}}{\rho}}\right)k \Rightarrow c_T = \sqrt{\frac{c_{44}}{\rho}}\right\}$$
(4)

Note that there is only one unique shear wave speed in the axial (A) principal direction, and these speeds correspond to group velocities as these dispersion relations are linear in k. Similarly, the dispersion relations in each radial (R) (major ( $R_1$ ) or minor ( $R_2$ )) direction (Fig. 1.b) are obtained for one pressure (L) and two distinct shear (T) modes. The corresponding phase speeds (one pressure and two distinct shear speeds) in the radial (R) major (1) directions (1, 0, 0) are as follows:

$$\left\{\omega = \pm \left(\sqrt{\frac{c_{11}}{\rho}}\right)k \Rightarrow c_L = \sqrt{\frac{c_{11}}{\rho}}\right\}$$

$$\left\{\omega = \pm \left(\sqrt{\frac{c_{44}}{\rho}}\right)k \Rightarrow c_T = \sqrt{\frac{c_{44}}{\rho}}\right\}$$

$$\left\{\omega = \pm \left(\sqrt{\frac{c_{66}}{\rho}}\right)k \Rightarrow c_T = \sqrt{\frac{c_{66}}{\rho}}\right\}$$
(5)

In the tiso case, these speeds are identical for the direction along the major (1, 0, 0) and minor (0, 1, 0) principal directions.

From these two sets of equations, if the four unique pressure and shear speeds along the principal axes (namely, axial (z) and (major (x)and minor (y)) radial) are obtained, we can extract  $c_{11}$ ,  $c_{33}$ ,  $c_{44}$ , and  $c_{66}$ , but not  $c_{13}$  since it is absent in these velocity expressions (Eqs. (4) and (5)). Thus, an additional dispersion equation is needed for the determination of  $c_{13}$ . It is noteworthy that  $c_{13}$  is not needed to extract  $c_{11}$ ,  $c_{33}$ ,  $c_{44}$ , and  $c_{66}$ . In the reported experiments, for the extraction of  $c_{13}$ , additional speed measurements in a third direction, which is different from the principal axes (see the slowness diagram in Fig. 2.a), are required. Slowness is the inverse of velocity. As shown below, such a direction (projected to  $R_1$  and A on the  $R_1$ -A plane) for an oblong tablet is taken as  $(\cos(\varepsilon), 0, -\sin(\varepsilon))$  for an angle of  $\varepsilon$  between the propagation direction and the axis  $R_1$  as shown in Fig. 1.b. If  $\varepsilon$  is a small angle (in radians), the propagation direction is approximated by using Taylor series expansions around  $\varepsilon = 0$  as  $\cos(\varepsilon) \sim 1$ -  $\varepsilon^2/2 + \varepsilon^4/24 + O(\varepsilon^5)$  and  $\sin(\varepsilon) \sim \varepsilon - \varepsilon^3/6 + O(\varepsilon^4)$ . The numerical values for the polynomial terms used in the following analysis are included to indicate the convergence accuracy of these trigonometric expansions as follows:

$$\varepsilon = 9.82^{\circ} = 0.17139 \, \text{rad sin}(\varepsilon) = 0.170553$$

$$1 - \frac{\varepsilon^2}{2} = 0.985313 \cos(\varepsilon) = 0.985348 \tag{6}$$

$$\varepsilon^2/2 = 0.0146875 \ \varepsilon^3/6 = 0.000831 \ \varepsilon^4/24 = 0.00003593$$

For the off-major axis (1) direction,  $(\cos(\varepsilon), 0, -\sin(\varepsilon)) \sim (1-\varepsilon^2/2, 0, -\varepsilon)$ , from the Christoffel equation, with the help of Mathematica®, we approximate the three branches of the dispersion relation and the corresponding three-wave speeds (pressure (axial (A), z) and two shear components with polarization in  $\times$  (major  $(R_1)$ ) and y (minor  $(R_2)$ ) directions (Fig. 1.b) as follows:

$$\omega = \left(\pm \sqrt{\frac{c_{11}}{\rho}} \pm \frac{((c_{11} + c_{13}) (c_{11} - c_{13} - 2c_{44}))}{2\sqrt{\rho c_{11}} (c_{44} - c_{11})} \varepsilon^{2} + O(\varepsilon^{4})\right) k$$

$$\Rightarrow {}^{1}c_{L} = \pm \sqrt{\frac{c_{11}}{\rho}} \pm \frac{((c_{11} + c_{13}) (c_{11} - c_{13} - 2c_{44}))}{2\sqrt{\rho c_{11}} (c_{44} - c_{11})} \varepsilon^{2} + O(\varepsilon^{4})$$

$$\omega = \left(\pm \sqrt{\frac{c_{44}}{\rho}} \pm \frac{(c_{13} - c_{11} c_{33} + (c_{11} + 2c_{13} + c_{33}) c_{44})}{2\sqrt{\rho c_{44}} (c_{44} - c_{11})} \varepsilon^{2} + O(\varepsilon^{4})\right) k$$

$$\Rightarrow {}_{S}c_{T} = \pm \sqrt{\frac{c_{44}}{\rho}} \pm \frac{(c_{13} - c_{11} c_{33} + (c_{11} + 2c_{13} + c_{33}) c_{44})}{2\sqrt{\rho c_{44}} (c_{44} - c_{11})} \varepsilon^{2} + O(\varepsilon^{4})$$

$$\omega = \left(\pm \sqrt{\frac{c_{66}}{\rho}} \pm \frac{(c_{44} - c_{66})}{2\sqrt{\rho c_{66}}} \varepsilon^{2} + O(\varepsilon^{4})\right) k$$

$$\Rightarrow {}_{F}c_{T} = \pm \sqrt{\frac{c_{66}}{\rho}} \pm \frac{(c_{44} - c_{66})}{2\sqrt{\rho c_{66}}} \varepsilon^{2} + O(\varepsilon^{4})$$

$$(7)$$

Note that in these expressions, only two diagonal speeds (pressure  $^{1}c_{L}$  and slow shear  $_{S}c_{T}$ ) are dependent on  $c_{13}$ . The diagonal fast shear mode (F)  $_{F}c_{T}$  is independent of  $c_{13}$ . As the fastest wave component is the easiest to extract from a waveform, we use the first expression for  $^{1}c_{L}$  in the following analysis for determining  $c_{13}$ .

Solving the first equation for the longitudinal (pressure) speed component in Eq. (7) after setting it to the diagonally measured pressure speed (Fig. 1.b) at  $\varepsilon$ , to  $^{1}\varepsilon_{1}$ , namely,

$${}^{1}c_{L} = \pm \sqrt{\frac{c_{11}}{\rho}} \pm \frac{((c_{11} + c_{13})(c_{11} - c_{13} - 2c_{44}))}{2\sqrt{\rho c_{11}}(c_{44} - c_{11})} \varepsilon^{2} + O(\varepsilon^{4})$$
(8)

The extraction of  $c_{13}$  from Eq. (8) with this small propagation angle  $\varepsilon$  yields:

$$c_{13} = \frac{1}{\varepsilon} \sqrt{(c_{11} - c_{44})(-2c_{11} + (c_{11} - c_{44})\varepsilon^2 + 2^{-1}c_L\sqrt{\rho c_{11}})} - c_{44}$$
 (9)

This closed-form approximation is utilized in the experimental work detailed below. For large propagation angles, the direct numerical solution of the Christoffel equation is required and adopted.

## 3. Materials and methods

Commercially available over-the-counter Acetaminophen tablets from Amazon Basic Care (ASIN: B074F2H9VT) (manufactured by Perrigo Co. Inc., Allegan, Michigan, USA) were adopted in the experimental studies reported in the current work (Fig. 1.a). Ten samples were randomly selected (referred to as ACE) for experiments from a bottle of 200 tablets with a lot number of 1GV1946. These tablets were high-aspect-ratio oblong-shaped, white-colored, with embossed code L484 and produced by compaction along the axial direction only; as a result, transversely isotropic elastic properties were developed. The active pharmaceutical ingredient (API) of the ACE tablets was Acetaminophen (500 mg), which is widely consumed to relieve pain and fever. Other ingredients (inactive excipients and additives) included carnauba wax, cornstarch, croscarmellose sodium, hypromellose, polyethylene glycol,

**Table 1** The measured average compact thicknesses in the axial  $(h^A)$ , radial major  $(^1h^R)$ , diagonal major  $(^1h^D)$ , radial minor  $(^2h^R)$ , diagonal minor  $(^2h^D)$ , mass  $(m_A)$ , apparent mass density  $(\rho_A)$  with their averages, SDs, and percentage of SDs for the ACE sample set.

Measured Physical Parameters of the ACE Sample Set									
Sample No.	h <sup>A</sup> (mm)	<sup>1</sup> h <sup>R</sup> (mm)	<sup>1</sup> h <sup>D</sup> (mm)	<sup>2</sup> h <sup>R</sup> (mm)	<sup>2</sup> h <sup>D</sup> (mm)	m <sub>A</sub> (mg)	$\frac{\rho_A}{(\text{kg/m}^3)}$		
1 2 3 4 5 6 7 8	5.13 5.12 5.17 5.18 5.19 5.20 5.11 5.18 5.13	17.50 17.47 17.50 17.50 17.52 17.53 17.46 17.46	17.20 17.47 17.59 17.42 17.52 17.49 17.40 17.34 17.50	7.15 7.19 7.15 7.16 7.16 7.18 7.15 7.16 7.16	7.68 7.72 7.67 7.69 7.65 7.69 7.68 7.70 7.69	555.90 548.50 551.80 555.40 555.90 562.00 553.00 555.50 545.90	1057.19 1034.11 1041.37 1050.84 1045.89 1053.60 1058.23 1045.75 1034.37		
10 Avg SD	5.15 5.16 0.03	17.51 17.49 0.03	17.41 17.43 0.11	7.16 7.16 0.01	7.72 7.69 0.02	551.70 553.56 4.48	1044.59 1046.59 8.52		
% SD	0.62	0.15	0.62	0.18	0.28	0.81	0.81		

povidone, pregelatinized starch, sodium starch glycolate, and stearic acid. The apparent mass density ( $\rho_A=m_A/V$ ) of the samples was evaluated by measuring dimensions with CD-6 in CS Absolute Digimatic Caliper (Mitutoyo Inc., Aurora, IL, USA), which was employed in SolidWorks 2020 (Dassault Systèmes SolidWorks Corporation, Waltham, MA, USA) for obtaining the volume and sample masses are measured by a digital scale (Model: A120S-L, Mettler-Toledo Inc., Columbus, Ohio, USA). The ACE sample set had an average mass of 550.00 mg and an average apparent density of 1046.59 kg/m³. The detailed shape of the sample set ACE tablets is illustrated in Fig. 1.a-b, and their geometric dimensions, masses, and mass densities are reported in Table 1.

## 4. Experimental set-up and waveform acquisition

In the reported experiments, a robotized and semi-automated rig experimental set-up (CTF 2022 system, Pharmacoustics Technologies, LLC, Potsdam, New York, USA) was customized along with the commonly used experimental set-up (ATT 2020 system, Pharmacoustics Technologies, LLC, Potsdam, New York, USA) for improving the measurement repeatability, accuracy and the reliability of non-destructive ultrasonic characterization. Ultrasonic pressure and shear experiments were executed in five different directions (axial, radial major, radial major diagonal, radial minor, and radial minor diagonal) of the ACE sample set. CTF 2022 was introduced to extract data for the axial and radial-minor direction of the compacts, while ATT 2020 was

incorporated for the radial-major and cross-diagonal orientation because of the complexity of tablet handling.

For data acquisition and analysis LabVIEW 2015 (National Instruments Corp., Austin, Texas, USA) software-based graphical user interface (GUI) (Ultrasonic Measurement Instrument (UMI 2022), Pharmacoustics Technologies, LLC, Potsdam, New York, USA) was developed. The CTF 2022 consists of a collaborative robot (UR3e, Universal Robots, Odense S, Denmark) with a payload of 6 lb, a vibratory bowl feeder (Model 5, Automation Devices Inc., Fairview, Pennsylvania, USA), a piezoelectric in-line feeder (L60A, Sanki Engineering CO., LTD, Tokyo, Japan), a stepper motor with a linear guide system (RGS04, Haydon Kerk, Waterbury, Connecticut, USA) for compacts feeding, two pressure (compression) transducers (V540-SM, Olympus Corporation, Center Valley, Pennsylvania, USA) with a central frequency of 2.25 MHz, two shear (transverse wave) transducers (V154-RM, Olympus Corporation, Center Valley, Pennsylvania, USA) with a central frequency of 1 MHz, a pair of low attenuation delay-lines. The CTF 2022 set-up can be operated in both pitch-catch (transmission) and pulse-echo (reflection) modes for both pressure and shear waveforms. The working ultrasonic measurement principle of CTF 2022 is equivalent to that of ATT 2020, but the CTF 2022 rig has its own semi-autonomous tablet feeding and position mechanisms.

In this study, both the CTF 2022 and the ATT 2020 rig set-ups were utilized in the pitch-catch mode. The pulser/receiver parameters were set at a pulse width of 200 ns, pulse voltage of 350 V, a sampling rate of 100 MHz, an amplification gain of 10 dB, and an averaging (oversampling) rate of 512. In CTF 2022, the pulser-out pressure and shear transducer with the delayline (to separate the initial acoustic pulse (main bang) from the interface reflections inside the compacts by creating a time-lapse) were coupled with the end effector of the collaborative robot. The receiving pressure and shear transducers were mounted on the receiving pressure and shear station. A vibratory bowl feeder, a piezoelectric in-line feeder, and a stepper motor with the linear guide were introduced to continuously feed the compacts to the pressure and shear station from the production line and put sample compacts in the center of the receiving transducers. The pulser-out pressure transducer coupled with the delayline was vertically placed and centered in contact with the top surface of the compact automatically by the collaborative robot and exerting a constant axial load on the compact. An electrical pulse was generated by the ultrasonic signal generator (US Ultratek, PCIUT3100, Concord, CA, USA) which excited the pitching pressure transducer. The pressure (longitudinal) wave pulse was transmitted through the delayline, and the compact, which was placed on the surface of the receiving pressure transducer. Finally, the ultrasonic pulse is sensed by the receiving pressure transducer for investigating the ToF

**Table 2** The measured and calculated acoustically extracted parameters: Time-of-Flight  $(ToF_L, ToF_T, {}^1ToF_L, {}^1ToF_T, {}^1ToF_T, {}^1ToF_L)$  for pressure (L) and shear (T) waves in axial (A), radial (R) major (1), and diagonal (D) major (1) direction, corresponding pressure and (fast (F) and slow (S) modes) shear wave speeds  $(c_L, c_T, {}^1c_L, {}^1_Fc_T, {}^1_Sc_T)$  and  ${}^1c_L$  with their averages, SDs, and percentage of SDs for the ACE sample set.

Measured and Calculated Parameters of the ACE Sample Set in Both Axial and Radial-Major Directions												
Sample No.	$ToF_L$ (µsec)	$ToF_T$ (µsec)	$^{1}ToF_{L}$ (µsec)	$_{F}^{1}ToF_{T}$ (µsec)	$_{S}^{1}ToF_{T}$ (µsec)	$^{1}ToF_{L}$ (µsec)	c <sub>L</sub> (m/sec)	c <sub>T</sub> (m/sec)	<sup>1</sup> <i>c<sub>L</sub></i> (m/sec)	${}_{F}^{1}c_{T}$ (m/sec)	${}_{S}^{1}c_{T}$ (m/sec)	$c_L$ (m/sec)
1	3.15	5.12	8.28	13.83	15.61	8.01	1628.57	1001.95	2113.53	1265.37	1121.08	2147.32
2	3.10	5.15	8.01	14.14	16.28	8.13	1651.61	994.17	2181.02	1235.50	1073.10	2148.83
3	3.15	4.78	8.1	14.00	16.08	8.04	1641.27	1081.59	2160.49	1250.00	1088.31	2187.81
4	3.20	4.91	7.97	13.77	15.63	8.01	1618.75	1054.99	2195.73	1270.88	1119.64	2174.78
5	3.02	5.04	8	13.96	16.27	8.2	1718.54	1029.76	2190.00	1255.01	1076.83	2136.59
6	3.08	4.73	7.9	13.63	16.12	7.98	1688.31	1099.37	2218.99	1286.13	1087.47	2191.73
7	3.20	5.05	7.99	13.48	15.87	8.04	1596.88	1011.88	2185.23	1295.25	1100.19	2164.18
8	3.18	4.86	8	13.76	15.89	8.22	1628.93	1065.84	2182.50	1268.90	1098.80	2109.49
9	3.19	5.21	8.52	14.60	16.50	8.17	1608.15	984.64	2049.30	1195.89	1058.18	2141.98
10	3.18	4.83	8.04	13.88	15.93	8.05	1619.50	1066.25	2177.86	1261.53	1099.18	2162.73
Avg	3.15	4.97	8.08	13.91	16.02	8.09	1640.05	1039.05	2165.47	1258.45	1092.28	2156.54
SD	0.06	0.17	0.18	0.31	0.29	0.09	37.47	39.91	49.08	27.82	19.83	24.98
% SD	1.91	3.37	2.28	2.21	1.79	1.08	2.28	3.84	2.27	2.21	1.82	1.16

Table 3

The measured and calculated acoustically extracted parameters: Time-of-Flight  $(ToF_L, ToF_T, {}^2ToF_L, {}^2ToF_L, {}^2ToF_T, {}^2ToF_L)$  for pressure (L) and shear (T) waves in axial (A), radial (R) minor (R), and diagonal (R) minor (R) direction, corresponding pressure and (fast (R) and slow (R) modes) shear wave speeds (R), R0, and R2, R1, with their averages, SDs, and percentage of SDs for the ACE sample set.

Measured and Calculated Parameters of the ACE Sample Set in Radial-Minor Directions									
Sample No.	$^2ToF_L$ (µsec)	$_F^2 ToF_T$ (µsec)	${}_{S}^{2}ToF_{T}$ (µsec)	$^2ToF_L$ (µsec)	$^{2}c_{L}$ (m/sec)	$_F^2 c_T$ (m/sec)	$\frac{2}{s}c_T$ (m/sec)	$c_L$ (m/sec)	
1	3.26	5.49	6.37	3.50	2193.25	1302.37	1122.45	2194.29	
2	3.42	5.73	6.51	3.73	2102.34	1254.80	1104.45	2069.71	
3	3.36	5.82	6.50	3.67	2127.98	1228.52	1100.00	2089.92	
4	3.21	5.64	6.41	3.63	2230.53	1269.50	1117.00	2118.46	
5	3.30	5.74	6.59	3.76	2169.70	1247.39	1086.49	2034.57	
6	3.25	5.85	6.70	3.59	2209.23	1227.35	1071.64	2142.06	
7	3.21	5.62	6.31	3.55	2227.41	1272.24	1133.12	2163.38	
8	3.25	5.66	6.40	3.57	2203.08	1265.02	1118.75	2156.86	
9	3.37	5.58	6.47	3.72	2124.63	1283.15	1106.65	2067.20	
10	3.35	5.71	6.42	3.67	2137.31	1253.94	1115.26	2103.54	
Avg	3.30	5.68	6.47	3.64	2172.55	1260.43	1107.58	2114.00	
SD	0.07	0.11	0.11	0.09	46.60	23.27	18.11	50.20	
% SD	2.22	1.92	1.76	2.35	2.14	1.85	1.63	2.37	

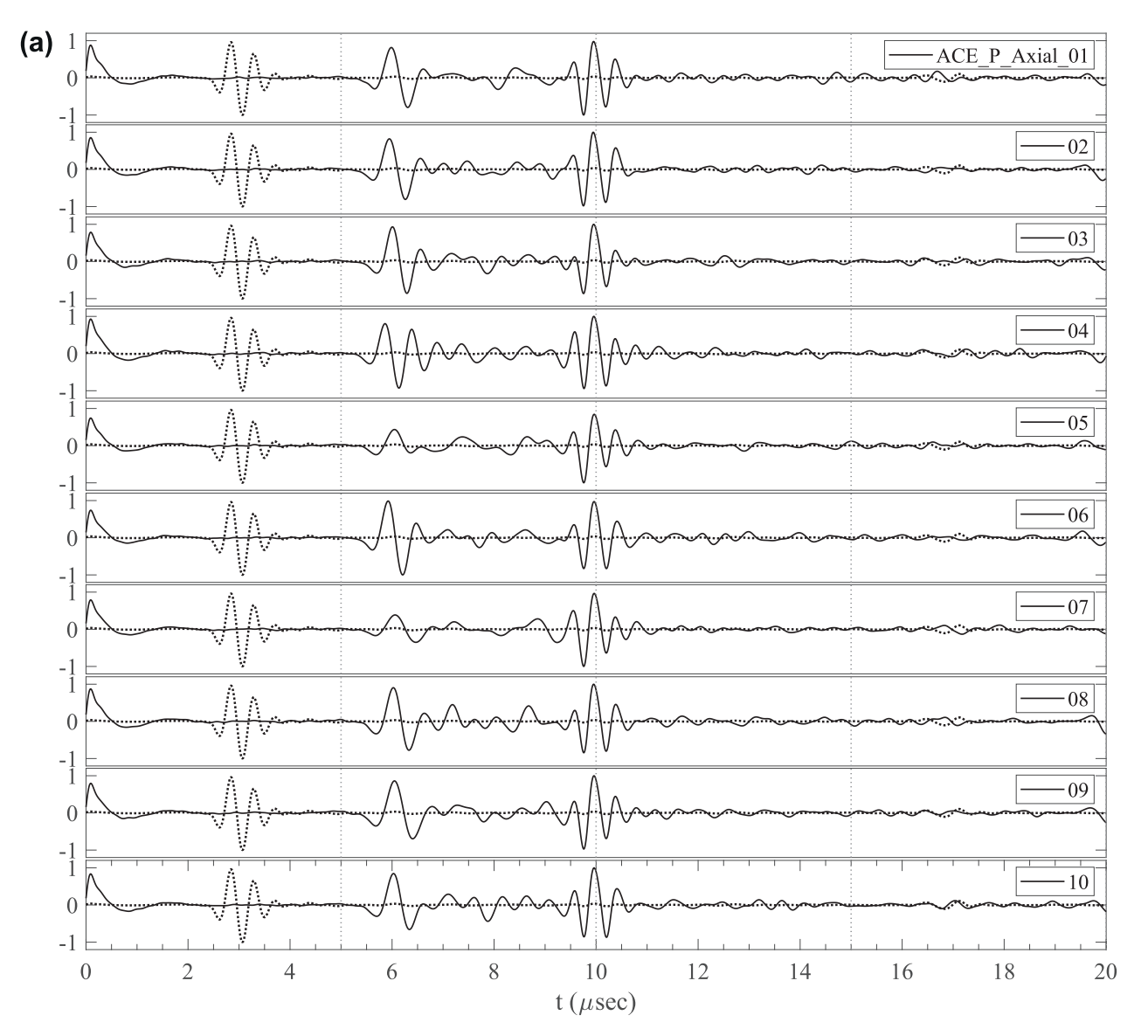


**Fig. 3.** Normalized pressure waveforms in (a) the axial (A), (c) radial (R) major, (g) radial (R) minor, (f) radial (R) major diagonal (D), (j) radial (R) minor diagonal (D) direction, and shear waveforms in (b) axial (A) (d-e) radial (R) major (fast (F) and slow (S) shear (T) speeds) (h-i) radial (R) minor (fast (F) and slow (S) modes) direction for the ACE sample set with the delay line waveform (dotted).

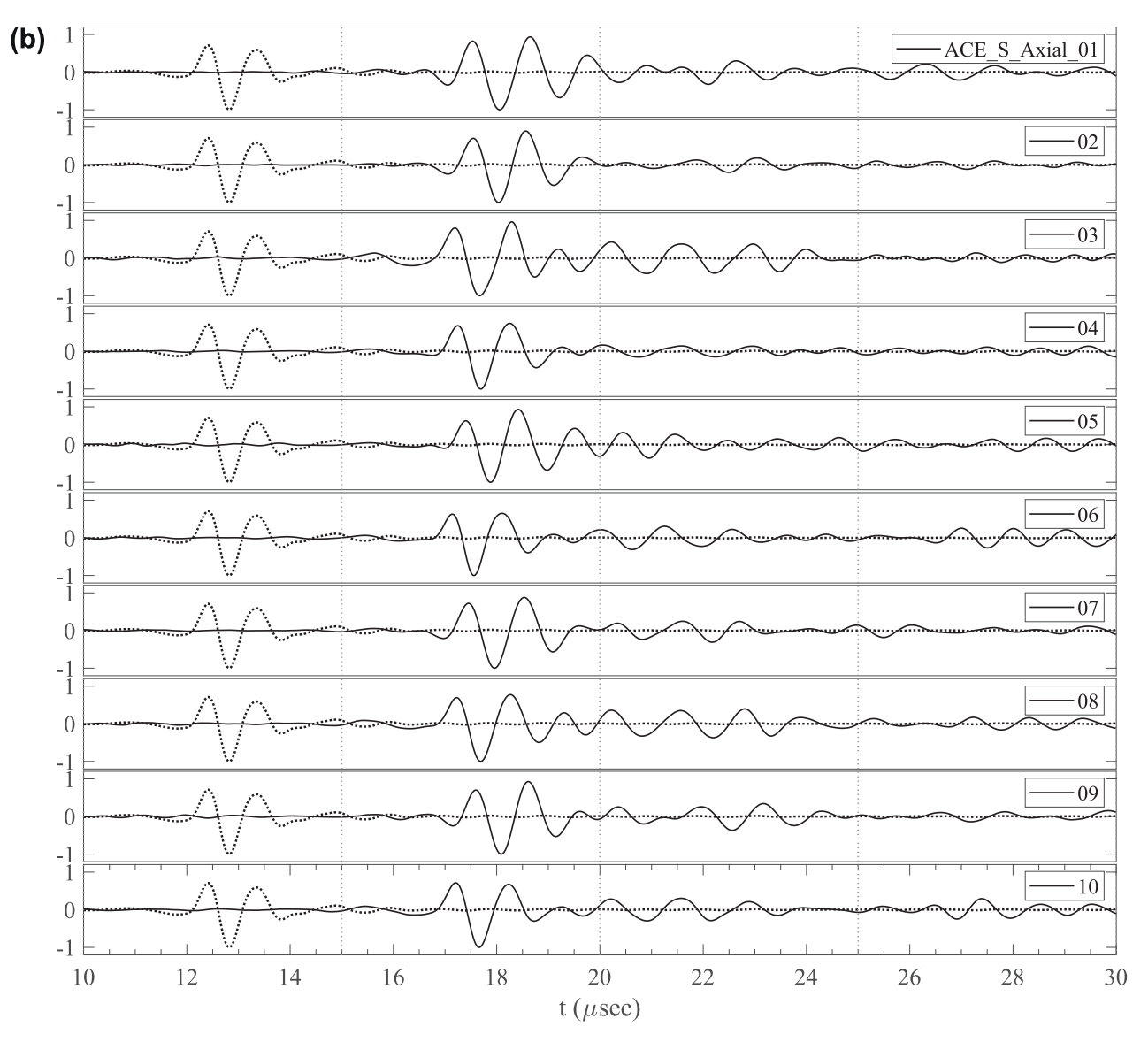


Fig. 3. (continued).

and the speed of sound using the UMI 2022 GUI. Once the data acquisition was complete, the stepper motor with the linear guide system placed the compact in a specific container depending on the quality. The same procedure was repeated using the shear transducer pair for the shear waveform acquisition.

On the other hand, during experiments with ATT 2020, each sample in major radial directions was placed on the bottom transducer manually, followed by the vertical movement of the top transducer to place it on top of the sample. Finally, the axial load was applied. During the experiments in a diagonal direction, the sample was held with a tablet holder to keep it stationary, and the slanted (diagonal) angle for the major axis was kept at  $\varepsilon=9.82^{\circ}$  and the minor axis at  $\alpha=22.82^{\circ}$  (illustrated in Fig. 2.c-d). In the ultrasonic tests, the applied load was set at 25  $\pm$  0.1 N to avoid deformation or change of microstructure while ensuring sufficient dry contact.

The acquired pressure (longitudinal) and shear (transverse) waveforms are processed to obtain the times-of-flight (ToF) determined by the peak-to-peak distance technique. For a tablet with a thickness of  ${}^Nh_X$ , the corresponding average wave speeds  ${}^N_Mc_X$  are calculated as:

$${}_{M}^{N}c_{X} = \frac{{}_{M}^{N}h_{X}}{{}_{M}^{N}ToF_{X}}$$

$$\tag{10}$$

where X = L (longitudinal, pressure) or T (transverse, shear), Y = A (axial) or R (radial) or D (cross – diagonal), M = F (fast mode) or S (slow mode) or blank when a single mode is propagated, and N = 1 (major axis) or 2 (minor axis) or blank when the propagation direction is axial (A). Similarly, extracted ToF and speeds are coded and reported (Tables 2 and 3):  ${}_{M}^{N}$ ToF ${}_{N}^{N}$   ${}_{M}^{C}$  ${}_{N}^{E}$  ${}_{D}^{E}$ ToF ${}_{LT}$ , and  ${}_{E}^{E}$  ${}_{C}$  ${}_{LT}$ .

There are a total of five elastic coefficients for the ACE sample set because of their transversely isotropic nature which is determined from the wave speeds, density, and diagonal propagation angles. We acquired, signal-processed and normalized pressure and shear waveforms in five directions (axial (A), radial (R) along the major (1) and minor (2) axes, and two diagonal directions (D) from the major (1) and minor (2) axes) (see Fig. 1.b for the principal axes and acquisition orientations  $\varepsilon$ and  $\alpha$ ). Note that while  $\varepsilon$  is a small angle,  $\alpha$  is large, thus the series approximation does not hold and the Christoffel equation is required to be solved numerically. Each acquired waveform has a unique identifier as ACE\_X\_Y\_Z\_S\_n (consider this alternative notation: MACE01x  $^{12}_{FS}ACE01_{LT}$ ) where X standard for the propagation mode (P for pressure (L for longitudinal) and S for shear (T for transverse)), the Y\_Z pair the propagation direction (A for axial, R for radial or D for diagonal propagation axis) and Z the axis of measurement (major (1) or minor (2), no Z for axial direction), S for the speed of the propagating wave mode (slow

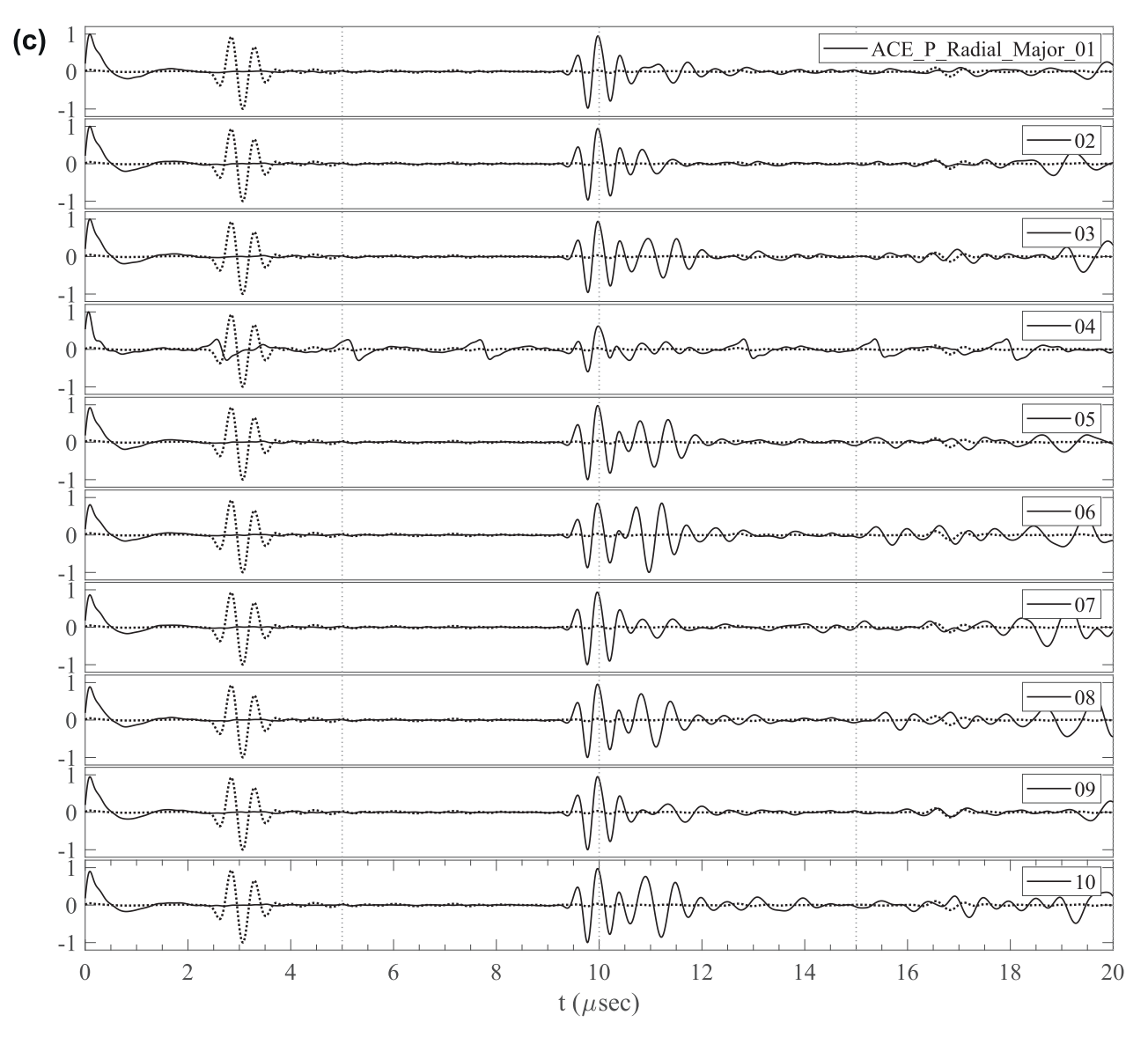


Fig. 3. (continued).

(*S*) or fast (*F*)), and *n* is the tablet number in the sample set (n = 1,...,10). For example, the waveform with the identifier of ACE\_P\_Radial\_Minor\_Diagonal\_03 indicates that the corresponding waveform (Fig. 3.*j*) is for the third ACE tablet in the sample set, the acquisition type is pressure (*P*), and the acquisition direction is along the minor (2) axis in the diagonal (*D*) orientation.

# 5. Results and discussions

Using the measured wave propagation speeds in the principal directions (reported in Tables 2 and 3 for the waveforms depicted in Fig. 3), we determine all [C] matrix components except  $c_{13}$  as follows:

$$c_L = {}^1c_L = \pm \sqrt{\frac{c_{11}}{\rho}} = 2165.47 \text{ m/s} \Rightarrow c_{11} = 4.90770 \text{ GPa}$$

$$c_L = {}^2c_L = \pm \sqrt{\frac{c_{11}}{\rho}} = 2172.55 \text{ m/s} \Rightarrow c_{11} = 4.93988 \text{ GPa}$$

$$c_L = c_L = \pm \sqrt{\frac{c_{33}}{\rho}} = 1640.05 \text{ m/s} \Rightarrow c_{33} = 2.81508 \text{ GPa}$$

$$c_T = {}_Sc_T = {}_Fc_T = \pm \sqrt{\frac{c_{44}}{\rho}} = 1039.05 \Rightarrow c_{44} = 1.12992 \text{ GPa}$$

$$c_T = {}_S^1c_T = \pm \sqrt{\frac{c_{44}}{\rho}} = 1092.28 \text{ m/s} \Rightarrow c_{44} = 1.24866 \text{ GPa}$$

$$c_T = {}_S^2c_T = \pm \sqrt{\frac{c_{44}}{\rho}} = 1107.58 \text{ m/s} \Rightarrow c_{44} = 1.28389 \text{ GPa}$$

$$c_T = {}_F^2c_T = \pm \sqrt{\frac{c_{66}}{\rho}} = 1258.45 \text{ m/s} \Rightarrow c_{66} = 1.65748 \text{ GPa}$$

$$c_T = {}_F^1c_T = \pm \sqrt{\frac{c_{66}}{\rho}} = 1253.94 \text{ m/s} \Rightarrow c_{66} = 1.6456 \text{ GPa}$$

Note that multiple values for the elastic coefficients except  $c_{33}$  are

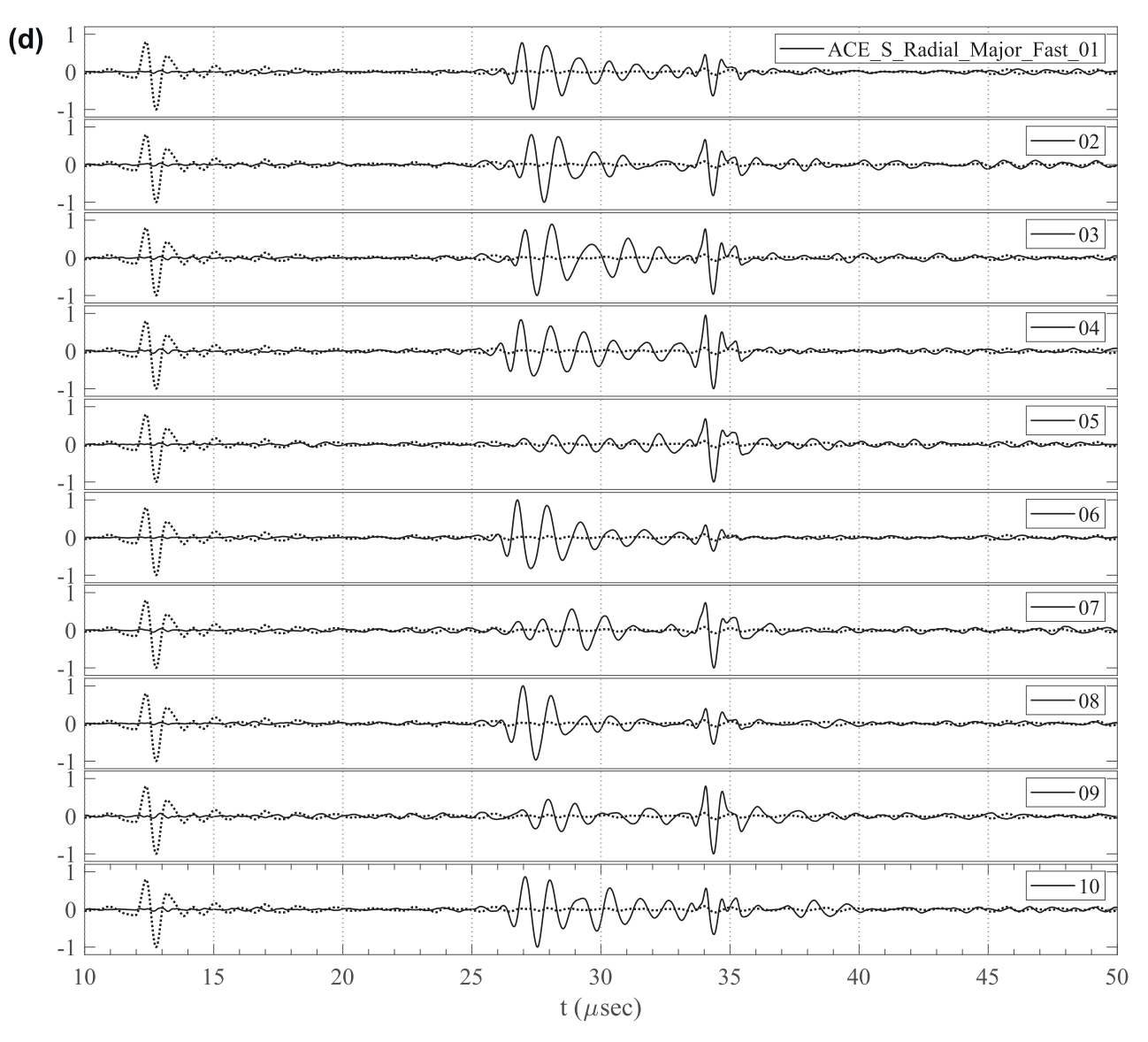


Fig. 3. (continued).

obtained, and some directional sensitivity is observed. We directly obtain  $c_{13}$  using Eq. (9) for  $\varepsilon$  (small angle), the diagonal pressure speed (2156.54 m/sec) from Table 2, and the extracted values of  $c_{13}, c_{33}, c_{44}$  and  $c_{66}$ :  $c_{13}=1.6054$  GPa. From the direct solution of the Christoffel equation for  $\alpha=22.9^{\circ}$  (large angle, so perturbation solutions do not apply) numerically, we also obtain  $c_{13}=1.5505$  GPa. The slight differences in the extracted values are attributed to either measurement inaccuracies and/or deviation from property axisymmetry in the radial axis.

Therefore, the complete constitutive matrix  $[C]^{\text{tiso}}$  for the ACE sample set is obtained as:

$$[C]^{tiso} = \begin{bmatrix} 4.9238 & 1.6036 & 1.5780 & 0 & 0 & 0\\ & 4.9238 & 1.5780 & 0 & 0 & 0\\ & & & 2.8115 & 0 & 0 & 0\\ & & & & 1.2196 & 0 & 0\\ & & & & & & 1.6601 \end{bmatrix} 10^{9} \text{Pa}$$

$$(12)$$

In Fig. 4, the evaluated wave speeds (Eq. 11) as a function of the sample orientation and wave propagation types along with the corresponding elastic coefficients in [C]<sup>tiso</sup>(Eq. 12) are shown. By setting Eq.

(12) to the tiso [*C*] values for the ACE tablet set in Eq. (3), we obtain the complete set of [*C*] matrix entries. The differences between the iso and tiso forms are determined as follows:

$$\begin{split} c_{44} + \Delta c_{66} &= c_{66} \Rightarrow \Delta c_{66} = c_{66} - c_{44} = 0.4404 \times 10^9 \Rightarrow \frac{\Delta c_{66}}{c_{44}} \\ &= 0.3611 = 36.1 \\ \% \ c_{11} + \Delta c_{33} = c_{33} \Rightarrow \Delta c_{33} = c_{33} - c_{11} \\ &= -2.1123 \times 10^9 \Rightarrow \frac{\Delta c_{33}}{c_{11}} = -0.4290 = -42.9 \\ \% \ c_{12} - 2\Delta c_{66} = c_{12} \Rightarrow c_{12} \\ &= c_{12} + 2\Delta c_{66} = 2.4845 \times 10^9 \ c_{12} + \Delta c_{13} = c_{13} \Rightarrow \Delta c_{13} = c_{13} - c_{12} \\ &= 0.9066 \times 10^9 \Rightarrow \frac{\Delta c_{13}}{c_{12}} = -0.3649 = -36.4 \\ \end{split}$$

These values indicate strong material anisotropy (21-42%) in the tablets adopted in this study as the variation ratios in Eq. (13) indicate.

In engineering notation, from Eq. (12), we set up the following matrix equation with the five unknowns  $E_1$ ,  $E_3$ , and  $G_{13}$ ,  $v_{12}$ , and  $v_{13}$  of the ACE tiso material (Meynard et al., 2021):

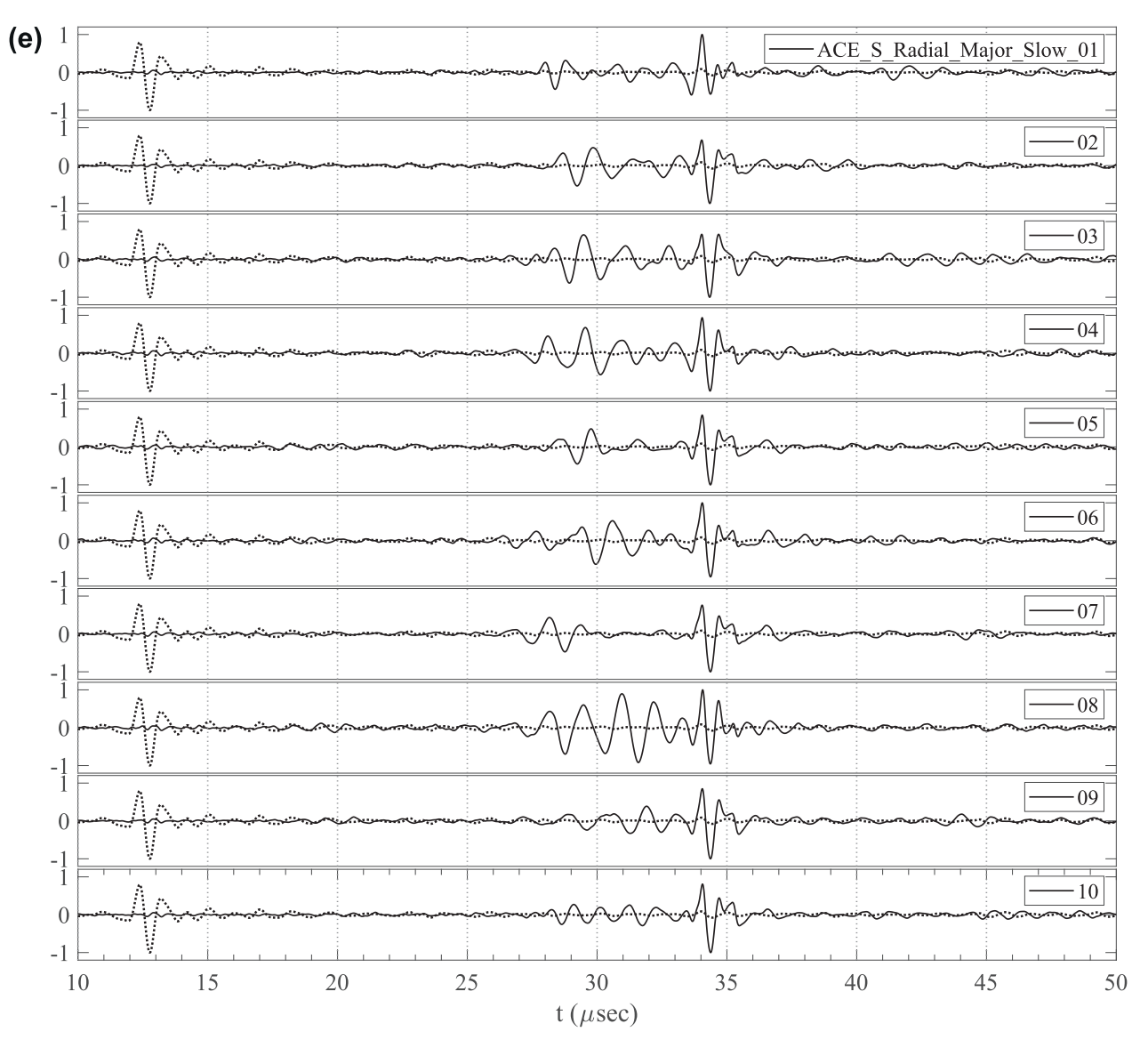


Fig. 3. (continued).

$$([C]^{tiso})^{-1} = \begin{bmatrix} 0.2557 & -0.0455 & -0.1180 & 0 & 0 & 0 \\ 0.2557 & -0.1180 & 0 & 0 & 0 \\ 0.4881 & 0 & 0 & 0 \\ 0.8199 & 0 & 0 \\ 0.8199 & 0 & 0 \\ 0.6024 \end{bmatrix} 10^{-9} \text{Pa}^{-1}$$

$$= \begin{bmatrix} 1/E_1 & -\nu_{12}/E_1 & -\nu_{13}/E_3 & 0 & 0 & 0 \\ 1/E_1 & -\nu_{13}/E_3 & 0 & 0 & 0 \\ 1/E_3 & 0 & 0 & 0 \\ 1/G_{13} & 0 & 0 \\ 0 & 1/G_{13} & 0 \\ 0 & 2(1+\nu_{12})/E_1 \end{bmatrix}$$

$$(14)$$

Solving this matrix equation (Eq. (14)) for the unknown variables we obtain the following elastic and shear moduli for the ACE tiso material: directional Young's moduli  $E_1 = E_2 = 3.9105$  GPa,  $E_3 = 2.0486$  GPa, and  $E_{13} = 1.2196$  GPa, and Poisson's ratios:  $E_{12} = 0.1778$ , and  $E_{13} = 0.2417$ . Based on the results of the previous experiments conducted with cubic

samples (Akseli et al., 2009),  $E_1 = E_2 = 3.9105$  GPa  $> E_3 = 2.0486$  GPa indicates that the elasticity of the tablet is mostly due to microcrystalline cellulose (MCC) in its formulation for increasing compressibility. In the lactose cubic samples, this order was found to be in reserve ( $E_1 = E_2 < E_3$ ), and in the ascorbic acid and aspartame cubic samples, no order was observed ( $E_1 = E_2 \approx E_3$ ) (Akseli et al., 2009).

## 6. Conclusions and remarks

A non-destructive ultrasonic approach for extracting the complete transverse isotropic elastic properties of high-aspect-ratio oblong-shaped compressed OSDFs is introduced. A mathematical framework is developed and presented to provide closed-form analytical solutions to extract the complete elastic parameters from the measured in-axis and off-axis propagation wave speeds. Also, a robotized and semi-automated rig experimental set-up (CTF 2022 system) is described and utilized along with the commonly used experimental set-up (ATT 2020 system) for automating and improving the measurement repeatability, accuracy, and the reliability of non-destructive ultrasonic evaluation and characterization of OSDFs.

In the reported experiments, the current characterization approach is applied to a commercially available over-the-counter oblong OSDF

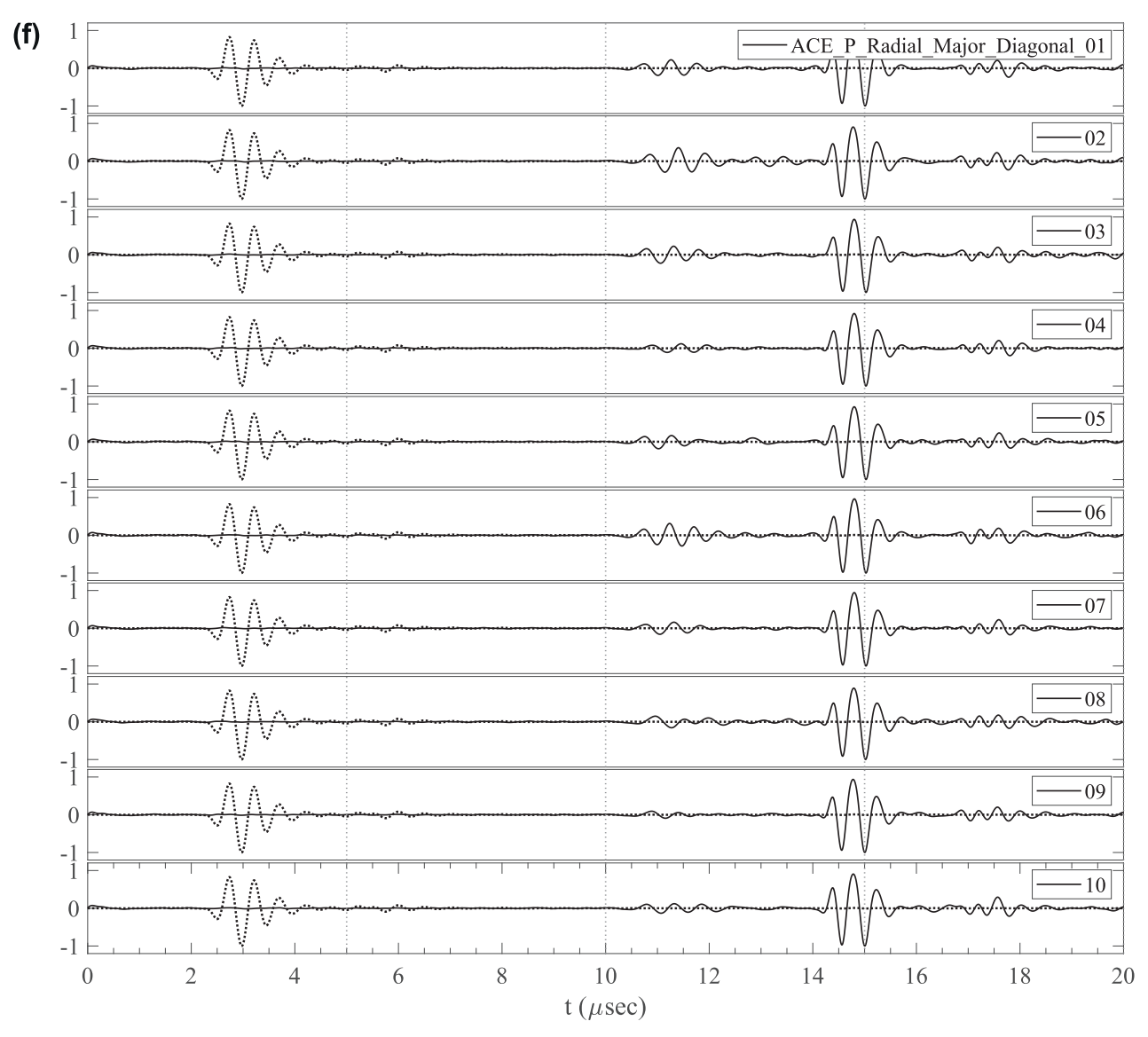


Fig. 3. (continued).

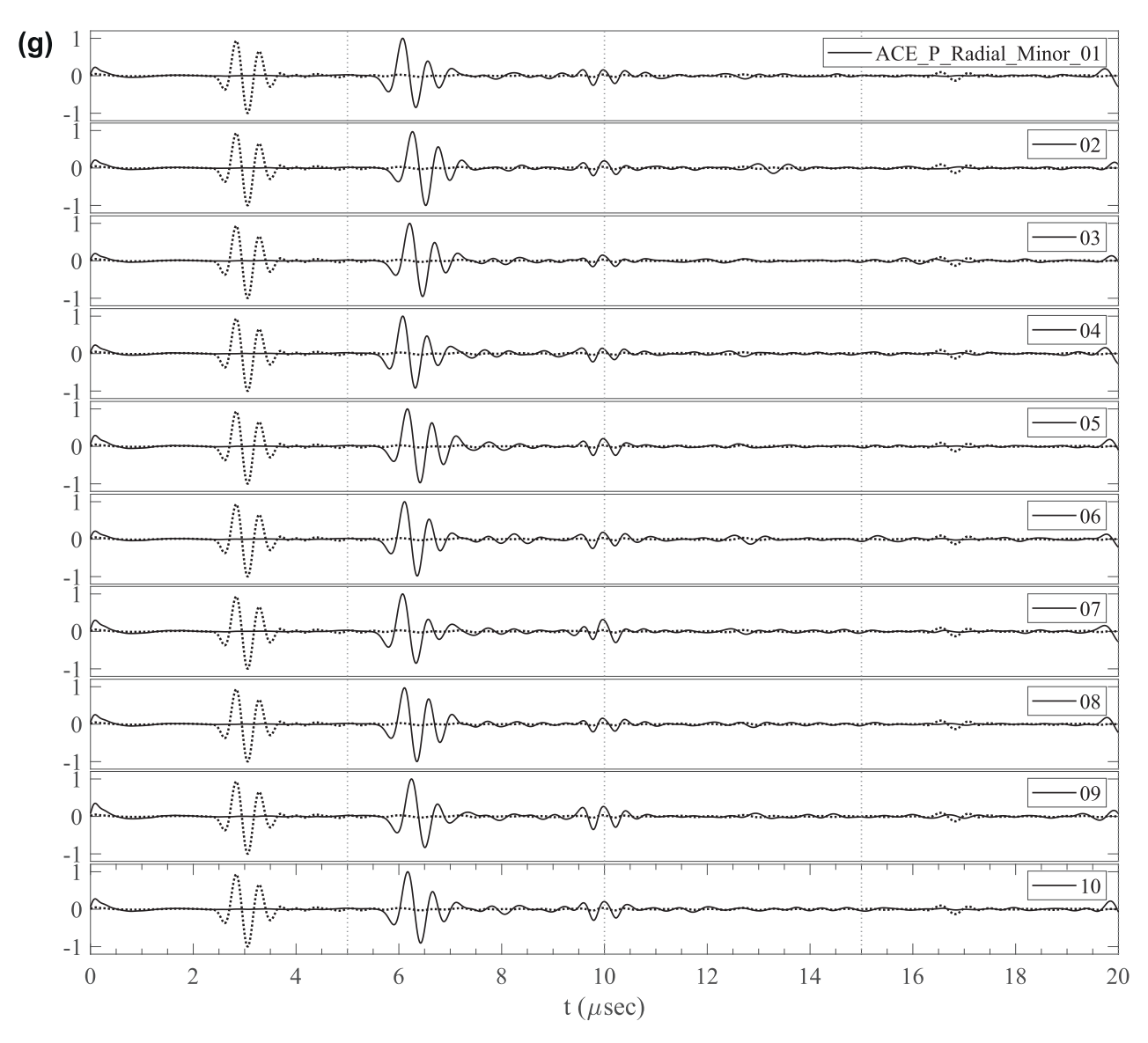


Fig. 3. (continued).

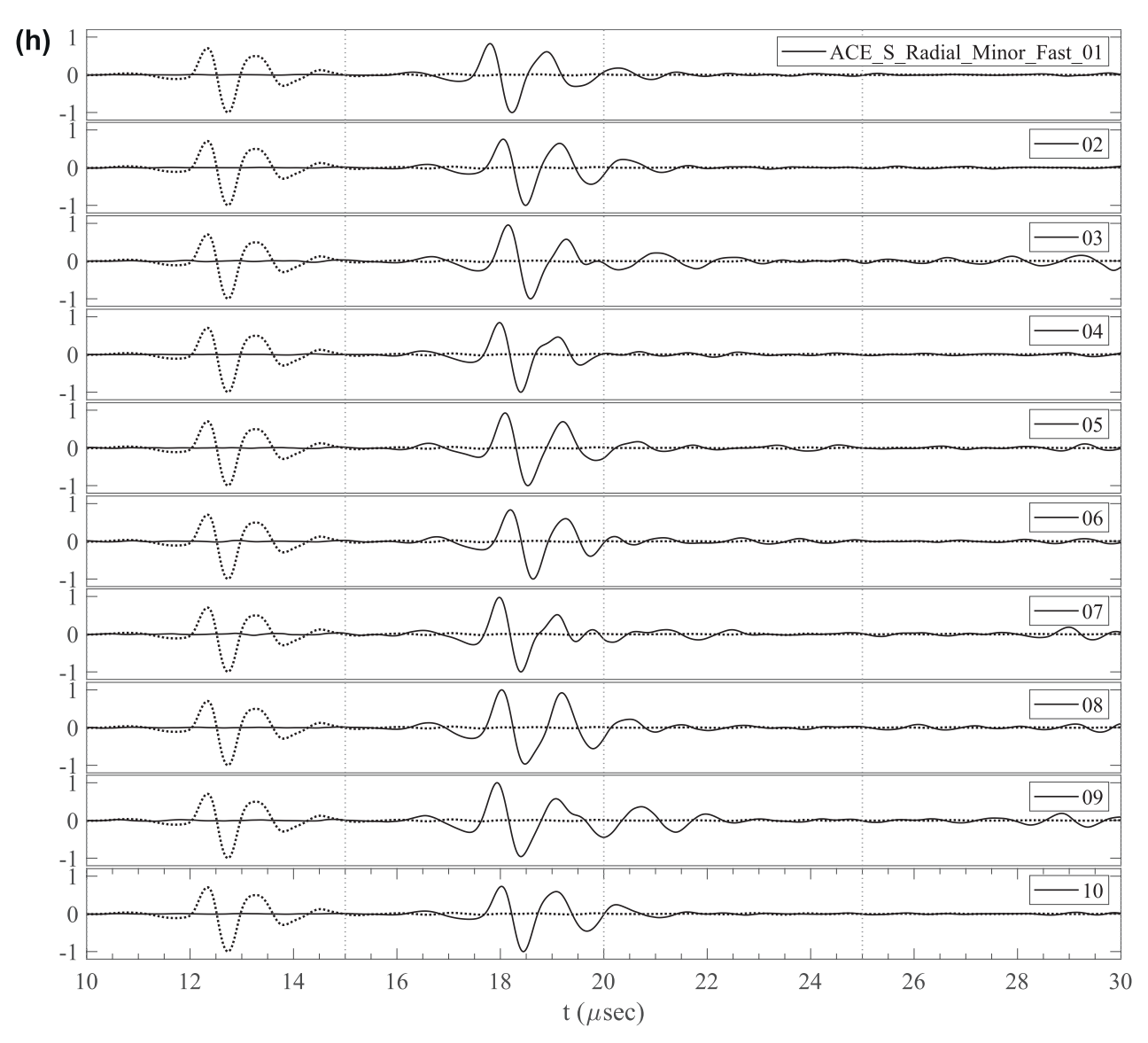


Fig. 3. (continued).

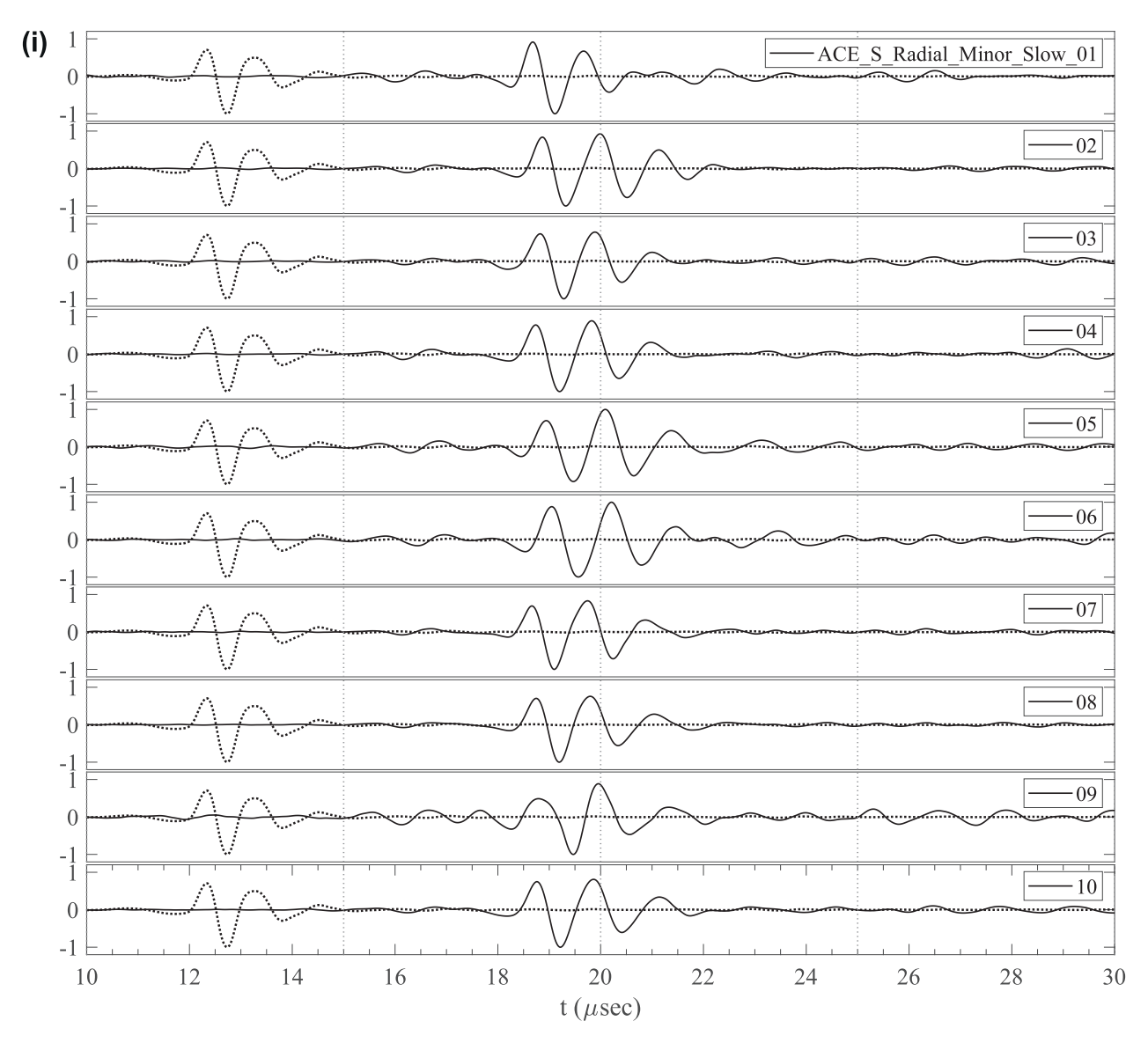


Fig. 3. (continued).

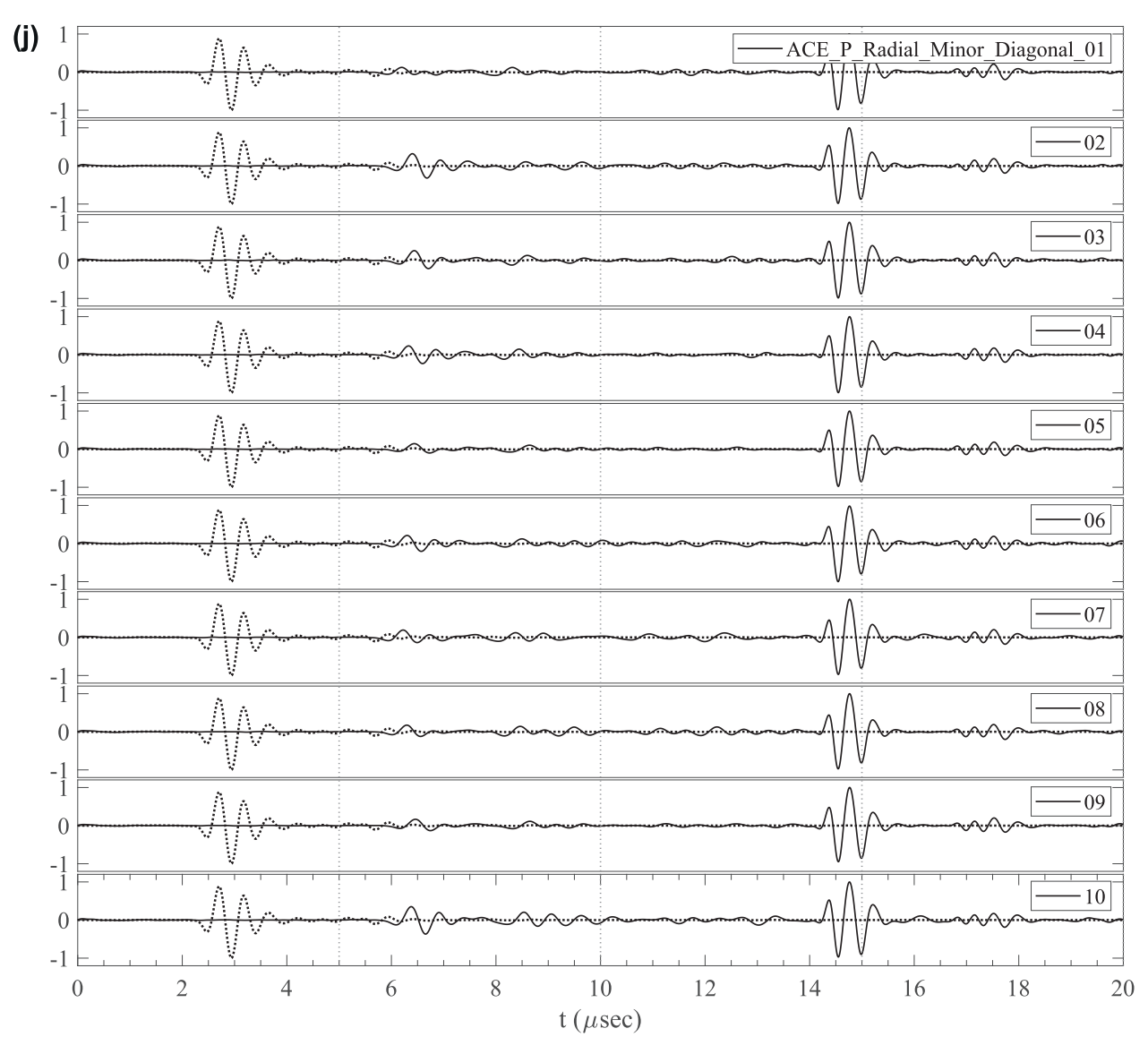
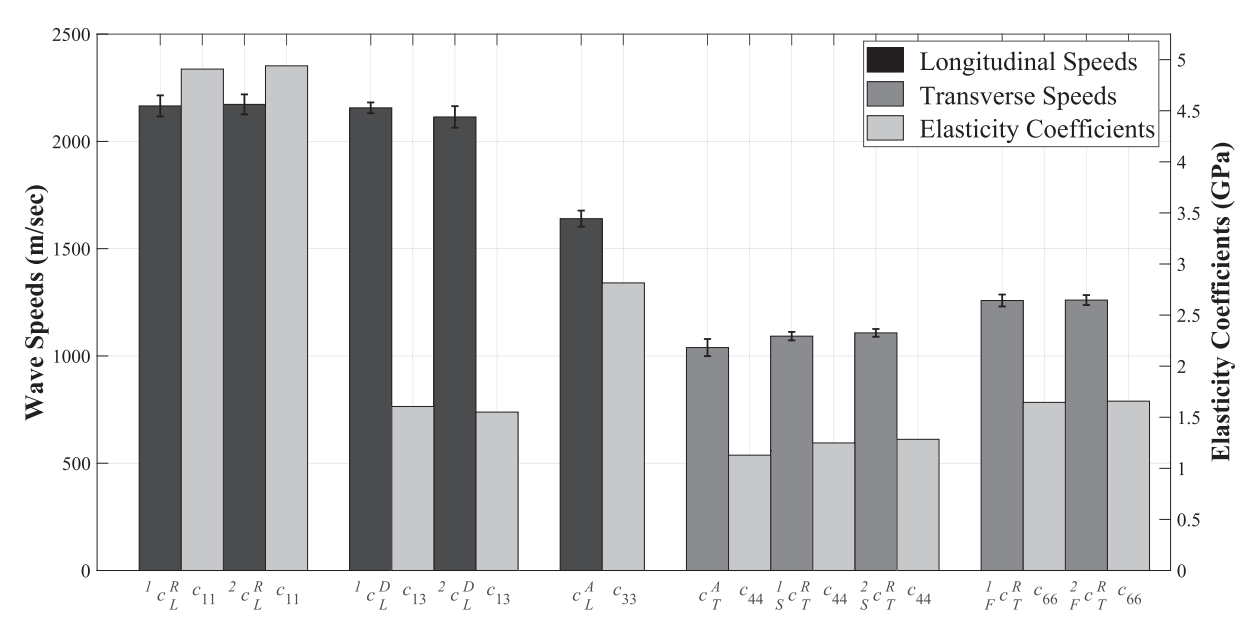


Fig. 3. (continued).



**Fig. 4.** The evaluated wave speeds as a function of the sample orientation (A, R, and D) and wave propagation types (L (longitudinal) and T (transverse)) (left side axis) along with the corresponding elastic coefficients in  $[C]^{tiso}$  (right-side axis).

product, and data sets, as well as the constitutive matrix for the tablet materials, are obtained and reported. The complete transverse isotropic elastic matrix requires five parameters:  $c_{11}$ ,  $c_{13}$ ,  $c_{33}$ ,  $c_{44}$ , and  $c_{66}$ , and only four elastic wave speeds in the principal coordinates of a compacted tablet can be acquired from time-of-flight information in two directions. Namely, with the measurements in the principal directions, all except  $c_{13}$  can be extracted. In the current work, we present and demonstrate how an additional ultrasonic measurement can be made, and its result is used to determine  $c_{13}$ , thus the complete set of elastic properties.

The engineering coefficients of the ACE tiso material were extracted, and it was found that  $E_1=E_2=3.9105~\mathrm{GPa}>E_3=2.0486~\mathrm{GPa},$  indicating the compressed materials are harder in the radial direction than in the major and minor axial directions. This observation can be counterintuitive as the tablet sample is compressed in the axial direction. The directional order of the Young's moduli values,  $E_1=E_2>E_3$ , indicates that the elasticity of the compressed tablet used in the experiments is dominated by the compressibility property of microcrystalline cellulose (MCC).

The demonstrated approach is a non-destructive, rapid, and reliable characterization technique to evaluate the anisotropy of compressed oral dosage forms.

## CRediT authorship contribution statement

**Tipu Sultan:** Formal analysis, Investigation, Visualization, Writing – review & editing. **Shubhajit Paul:** Supervision, Writing – review & editing. **Enamul Hasan Rozin:** Formal analysis, Investigation, Visualization, Writing – review & editing. **Christian Canino:** Investigation, Visualization. **Yin-Chao Tseng:** Supervision, Writing – review & editing. **Cetin Cetinkaya:** Conceptualization, Methodology, Software, Data curation, Writing – original draft, Supervision.

## **Declaration of Competing Interest**

The authors declare that they have no known competing financial interests or personal relationships that could have appeared to influence the work reported in this paper.

## Data availability

No data was used for the research described in the article.

#### Acknowledgements

The authors acknowledge funding from NSF STTR grant (Awards Number: 2051895) for automation and hardware development and Boehringer Ingelheim Pharmaceuticals, Inc. for the mathematical formulation, and Professor Vivek S. Dave of St. John Fisher College, Wegmans School of Pharmacy (Rochester, NY 14618, USA) for fruitful discussions on tablet design, development, and quality.

## References

Akseli, I., Cetinkaya, C., 2008. Air-coupled non-contact mechanical property determination of drug tablets. Int. J. Pharm. 359 (1-2), 25–34. https://doi.org/ 10.1016/j.ijpharm.2008.03.020.

Akseli, I., Dey, D., Cetinkaya, C., 2010. Mechanical Property Characterization of Bilayered Tablets using Non-destructive Air-Coupled Acoustics. AAPS PharmSciTech 11 (1), 90–102. https://doi.org/10.1208/s12249-009-9352-9.

Akseli, I., Hancock, B.C., Cetinkaya, C., 2009. Non-destructive determination of anisotropic mechanical properties of pharmaceutical solid dosage forms. Int. J. Pharm. 377 (1-2), 35–44. https://doi.org/10.1016/j.ijpharm.2009.04.040.

Akseli, I., Ladyzhynsky, N., Katz, J., He, X., 2013. Development of predictive tools to assess capping tendency of tablet formulations. Powder Technology, Special Issue: Pharmaceutical Powders 236, 139–148. https://doi.org/10.1016/j. powtec.2012.04.026.

Akseli, I., Stecula, A., He, X., Ladyzhynsky, N., 2014. Quantitative Correlation of the Effect of Process Conditions on the Capping Tendencies of Tablet Formulations. J. Pharm. Sci. 103 (6), 1652–1663. https://doi.org/10.1002/jps.23951.

Auld, B.A., 1990. Acoustic fields and waves in solids. Vol. II., 2. ed. ed. Krieger Publishing Company. Malabar. FL.

Baud, P., Louis, L., David, C., Rawling, G.C., Wong, T.-F., 2005. Effects of bedding and foliation on mechanical anisotropy, damage evolution and failure mode. Geological Society, London, Special Publications 245 (1), 223–249. https://doi.org/10.1144/ GSL.SP.2005.245.01.11.

Cetinkaya, C., 2014. Non-contact mechanical property determination of drug tablets. US8645084B1.

Cetinkaya, C., 2017. Methods and systems for in-and out-of-die monitoring and characterization of multi-component tablets and for detecting and monitoring stiction and tooling material modifications on punch and die surfaces. IIS9739753B2.

Cetinkaya, C., 2019. Methods and systems for in-and out-of-die monitoring and characterization of multi-component tablets and for detecting and monitoring stiction and tooling material modifications on punch and die surfaces. US10429352B2.

Kern, M., Riedel, T., Breitkreutz, J., 2022. Investigating key properties of model excipients and binary powder blends using ultrasonic in-die measurements on a compaction simulator. Int. J. Pharm. 613, 121381. https://doi.org/10.1016/j. iipharm.2021.121381.

Meynard, J., Amado-Becker, F., Tchoreloff, P., Mazel, V., 2021. Use of impulse excitation technique for the characterization of the elastic anisotropy of pharmaceutical tablets. Int. J. Pharm. 605, 120797. https://doi.org/10.1016/j.ijpharm.2021.120797.

- Mullarney, M.P., Hancock, B.C., 2006. Mechanical property anisotropy of pharmaceutical excipient compacts. Int. J. Pharm. 314 (1), 9–14. https://doi.org/ 10.1016/j.ijpharm.2005.12.052.
- Paul, S., Baranwal, Y., Tseng, Y.-C., 2021. An insight into predictive parameters of tablet capping by machine learning and multivariate tools. Int. J. Pharm. 599, 120439. https://doi.org/10.1016/j.ijpharm.2021.120439.
- Paul, S., Tseng, Y.-C., 2021. A semi-empirical model for estimation of flaw size in internally defective tablets. J. Pharm. Sci. 110 (6), 2340–2345. https://doi.org/ 10.1016/j.xphs.2021.02.032.
- Pitt, K.G., Heasley, M.G., 2013. Determination of the tensile strength of elongated tablets. Powder Technol. 238, 169–175.
- Razavi, S.M., Callegari, G., Drazer, G., Cuitino, A.M., 2016. Toward predicting tensile strength of pharmaceutical tablets by ultrasound measurement in continuous

- manufacturing. Int. J. Pharm. 507 (1-2), 83–89. https://doi.org/10.1016/j.iipharm.2016.04.064.
- Xu, X., Coskunturk, Y., Dave, V.S., Kuriyilel, J.V., Wright, M.F., Dave, R.H., Cetinkaya, C., 2020. Effects of compaction pressure, speed and punch head profile on the ultrasonically-extracted physical properties of pharmaceutical compacts. Int. J. Pharm. 575, 118993. https://doi.org/10.1016/j.ijpharm.2019.118993.
- Xu, X., Mack, C., Cleland, Z.J., Vallabh, C.K.P., Dave, V.S., Cetinkaya, C., 2018a. Correlation of solid dosage porosity and tensile strength with acoustically extracted mechanical properties. Int. J. Pharm. 542 (1-2), 153–163. https://doi.org/10.1016/ j.ijpharm.2018.03.018.
- Xu, X., Vallabh, C.K.P., Hoag, S.W., Dave, V.S., Cetinkaya, C., 2018b. Early detection of capping risk in pharmaceutical compacts. Int. J. Pharm. 553 (1-2), 338–348. https:// doi.org/10.1016/j.ijpharm.2018.10.052.